JOURNAL OF GEOPHYSICAL RESEARCH, VOL. 91, NO. D3, PAGES 4025-4046, MARCH 20, 1986

IONS IN THE MESOSPHERE AND LOWER THERMOSPHERE : A TWO-DIMENSIONAL MODEL

G. Brasseur and P. De Baets

Institut d'Aeronomie Spatiale de Belgique, B-1180 Brussels, Belgium

Abstract. The behavior of ions in the D and E regions is shown to exhibit large latitudinal and seasonal variations. These are due to the meridional transport of neutral species (NO, O, H_2O) which interact with ion chemistry, to temperature variations, and to differences in the solar input and in high-energy particle precipitation. This paper presents a two-dimensional model of the ion composition in the D and E regions, which shows that the lower ionosphere is clearly dynamically controlled. The importance of the latitudinal and seasonal dependence of the nitric oxide concentration is pointed out. The model also shows that noticeable changes in the meridional distribution of ions should be attributed to the variability in the solar irradiance and in the strength of particle precipitation in relation to the 11-year solar cycle.

Introduction

In recent years, considerable effort has been devoted to understanding physical and chemical processes occuring in the middle atmosphere. In situ observations, laboratory measurements, and the development of sophisticated numerical models have led to the identification of many key chemical processes occurring below the altitude of 100 km.

Neutral trace species have, for example, been shown to play a considerable role in the formation of both positive and negative ions as well as in conversion reactions involved in ionic chemistry. Since the pioneering work of Nicolet [1945], much work has been done to understand the key processes occurring in the D region of the ionosphere. It is now widely accepted that the formation of ions and electrons between 70 and 90 km is essentially due to the ionization of nitric oxide by solar radiation at Lyman α and that other neutral species, such as water vapor and atomic oxygen, play an important role in subsequent ionic conversion processes. The high variability of the NO distribution suggested by several observations [e.g., Meira, 1971; Zbinden et al., 1975; Tohmatsu and Iwagami, 1976; Baker et al., 1977; Swider, 1978; Beran and Bangert, 1979; Abdu and Batista, 1979, etc...] and by model calculations [Solomon et al., 1982a; Brasseur, 1984; Garcia and Solomon, 1983] as well as the variations in the densities of atomic oxygen and water vapor should be reflected in the concentration of ions and electrons in the D region. As pointed out, for example, by Danilov and Taubenheim [1983], although the lifetime of charged particles is quite short in the ionosphere, the D region will nevertheless be controlled by dynamical processes. Thus the seasonal and latitudinal variations of long-lived species, such as H_2O , $O(^3P)$, and particularly NO, should be reflected in the composition of the ionosphere.

Other parameters directly related to the ion chemistry are also expected to vary with latitude. This is the case for the precipitation of cosmic rays which constitutes the major source of ions below about 70 km. The corresponding ionization rate varies by more than a factor of 10 between the equator and the geomagnetic pole [Heaps, 1978]. Moreover, the equilibrium constants of the ionic reactions and consequently the ionospheric composition will be very much influenced by the latitudinal and seasonal variations in the temperature (Figure 1), which are particularly significant near the mesopause.

These considerations show the necessity of extending the previous one-dimensional model studies of the lower ionosphere to two-dimensional studies. The purpose of this paper is to apply for different latitudinal and seasonal conditions an ion scheme with the rate constants as they are known from laboratory studies. The temperature distribution and the required transport parameters as well as the meridional fields of the neutral species concentration will be prescribed as input data.

Distribution of the Neutral Species Concentration

The composition of the D region is directly sensitive to the local concentration of several long-lived trace species, such as water vapor, atomic oxygen, nitric oxide, and carbon dioxide. Other gases, such as ozone, nitrogen dioxide and atomic hydrogen, also play a role in the negative ion scheme. The meridional distribution of these species will not be discussed in this paper but only quoted as an input to the ion model. One should nevertheless note that these distributions are taken from a two-dimensional model [Brasseur et al., 1980; Brasseur, 1984] in which the concentration fields of the long-lived constituents are derived from continuity/transport equations between the altitudes of 40-100 km. The meridional transport of these species is parameterized, using eddy diffusion coefficients (K_{yy}, K_{yz}, and K_{zz}) suggested by Ebel, [1980] and mean wind components based on the values of Murgatroyd and Singleton [1961] and on the analysis of Johnson and Gottlieb [1973]. This parameterization of the zonally averaged transport is very crude, since for example it does not explicitly consider the effects of gravity wave breaking and tides, which are believed to play an important role in determining both the intensity of turbulent eddy diffusion

Paper number 5D0707.
0148-0227/86/005D-0707$05.00

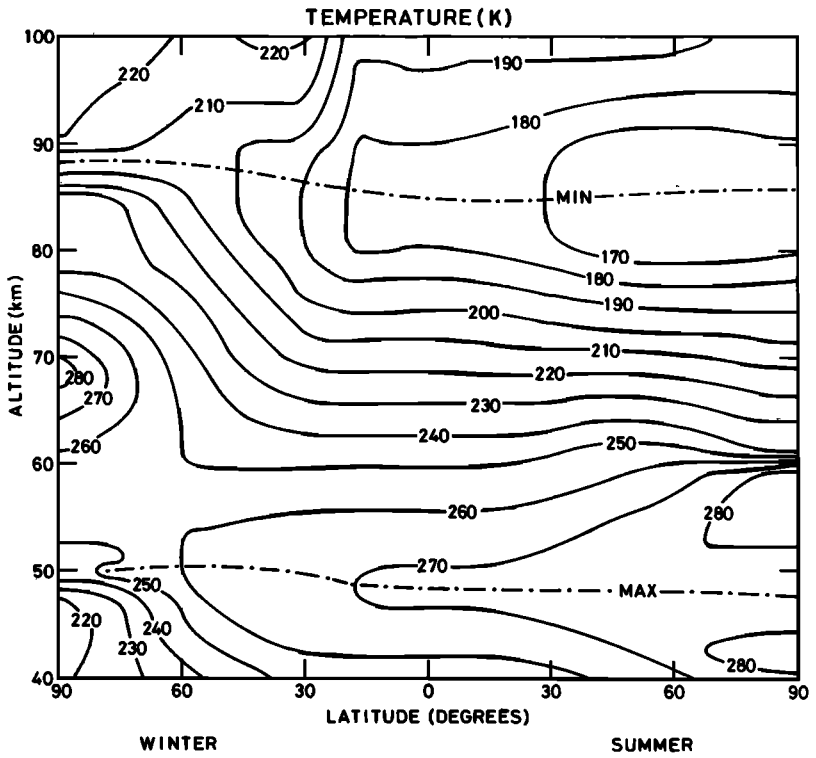

Fig. 1. Meridional distribution of the temperature (in Kelvin) adopted for a winter and a summer hemisphere, respectively.

and meridional advection in the mesosphere [Lindzen, 1981; Weinstock, 1982; Holton, 1983; Garcia and Solomon, 1985]. Nevertheless, the model with its adopted transport coefficients, provides distributions which are in reasonable agreement with available observations and predicts, for example, a significantly vigorous vertical transport in winter. Short-lived species are determined by assuming photochemical equilibrium conditions, while a uniform mixing ratio of 330 ppmv (parts per million by volume) is adopted for carbon dioxide.

Figure 2 presents the meridional distribution of the nitric oxide concentration, as adopted in the ion model. It can be seen that the concentration decreases gradually with altitude and reaches a minimum in the vicinity of the mesopause. This minimum is deepest in the summer hemisphere where the photodissociation of NO and the subsequent loss of odd nitrogen by recombination of $N(^4S)$ and NO is the most pronounced. The latitudinal dependence of the concentration minimum is enhanced by the strong variation of the mesopause temperature with latitude and season. During the summer the mesosphere is indeed particularly cold, leading to a small value of the rate constant of reaction

$$N(^4S) + O_2 \rightarrow NO + O$$

which competes with

$$N(^4S) + NO \rightarrow N_2O + O$$

and consequently to a larger odd nitrogen destruction. The meridional distribution of NO also depends on the adopted upper boundary condition particularly in winter when the vertical exchanges are strong. In this model we have adopted a given flux at 100 km altitude [S. Solomon, private communication, 1981], which corresponds to the net integrated production of nitric oxide above this level and takes into account, among other ionospheric processes, the effect of auroral particle precipitation.

The meridional distribution of the water vapor mixing ratio is displayed in Figure 3 which clearly shows that the behavior of this molecule is significantly different in summer and in winter.

Indeed, the behavior of H_2O results essentially from a transport from below, which is particularly strong in winter, and from a destruction by photolysis above 70 km, which is most efficient in summer. Differences in the mixing ratio between hemispheres of about a factor of 10 are obtained, indicating that the water vapor should be highly variable with the dynamical conditions and season [Grossmann, 1983].

The distribution of the atomic oxygen concentration is represented in Figure 4. The concentration increases rapidly above 75 km, where it becomes very sensitive to the magnitude of the transport parameters and to the prescribed upper boundary condition (a concentration of 5×10^{11} cm^{-3} and 3×10^{11} cm^{-3} in the winter and summer hemisphere, respectively). The vertical profiles of atomic oxygen, as given from Figure 4, are in good agreement, especially above 85 km, with a number of winter observations [Dickinson et al., 1974, 1976, 1985; Offermann et al., 1982] but do not reproduce the peak in concentration near 95 km observed at summer mid-latitudes. A smaller eddy diffusion coefficient (K_{zz}) in the lower

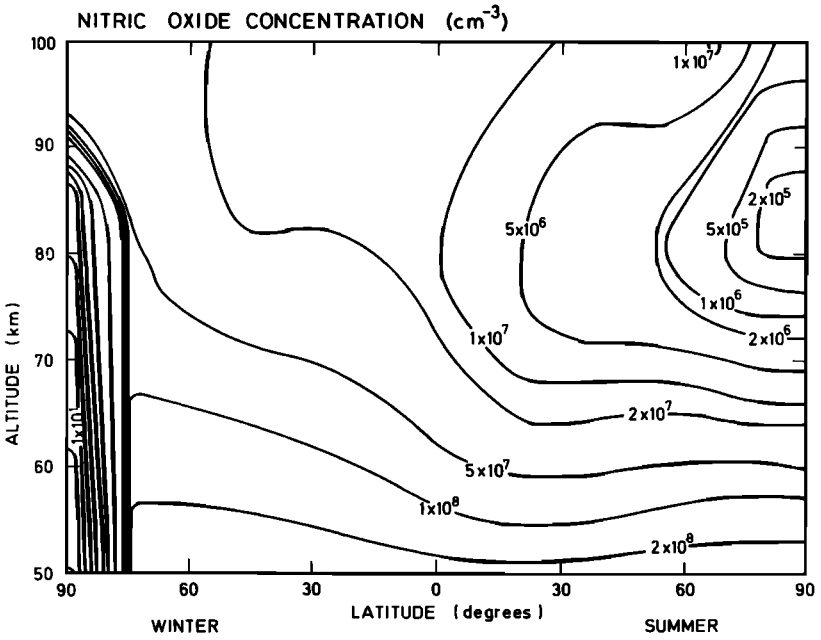

Fig. 2. Meridional distribution of the nitric oxide concentration (in cubic centimeters) adopted for a winter and summer hemisphere, respectively.

thermosphere, as suggested by Allen et al. [1981], with an appropriate flux as an upper boundary condition, may be used and tuned until the expected vertical atomic oxygen profile is obtained.

Ionospheric Chemistry and Model Description

The model used in the present study extends from 40 to 100 km altitude and therefore simulates not only the D region but also the lower part of the E region. Ionic concentrations are also calculated in the upper stratosphere, but in this latter region, which is characterized by the presence of non proton hydrates as positive ions and HSO_4^- cores as negative ions, the ionic chemistry has not been treated in detail. Most results will therefore be represented above 50 or 60 km. A model of positive and negative ions in the stratosphere has been developed by Brasseur and Chatel [1983], although many reaction rates applying to the chemical processes in this region are still very uncertain.

In the E region the ionization is due to the action of the EUV radiation. The primary ion N_2^+ is immediately converted into O_2^+ through a

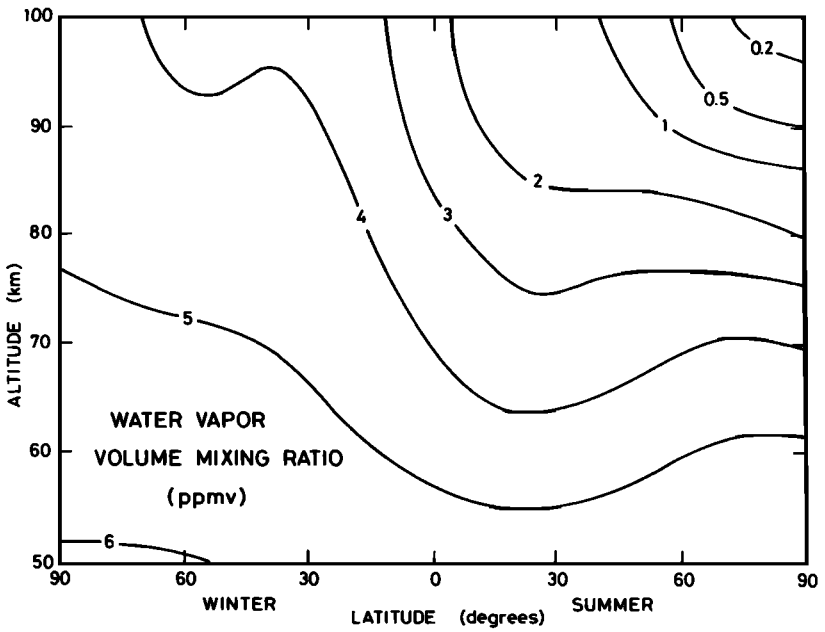

Fig. 3. Meridional distribution of the water vapor mixing ratio (ppmv) adopted for a winter and a summer hemisphere, respectively.

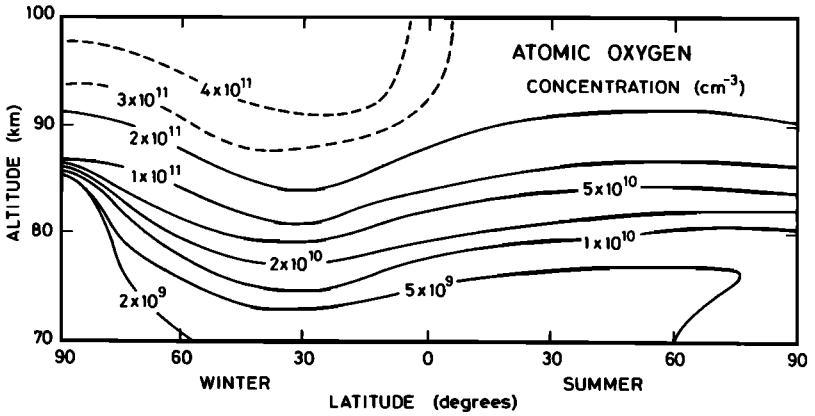

Fig. 4. Meridional distribution of the concentration of atomic oxygen (in cubic centimeters) between 70 and 100 km (24-hour average).

charge exchange with molecular oxygen. Moreover, NO^+ is produced by the reaction of N_2 with atomic oxygen or by the reaction of O_2 with nitric oxide. Both NO^+ and O_2^+, which are the major ions in the E region, recombine with electrons, the corresponding recombination rate being of the order of 2×10^{-7} cm^3 s^{-1}. The ionization rate of O_2, N_2, and O are calculated using the parameterization of Stewart [1970].

Metallic ions (Na^+, Mg^+, Al^+, Fe^+, Si^+) seem to be present in a permanent layer located around 95 km altitude and in some sporadic layers appearing above 100 km (see, e.g., Kopp and Herrmann [1984]). These ions, which are produced by meteoritic ablation, have not been considered in the present version of the model.

In the D region, as indicated previously, the major source of ionization is due to the action of the solar Lyman α line on the nitric oxide molecules. The calculation of this ionization rate has been performed using a cross-section value of 1.97×10^{-18} cm^2 for NO and 1×10^{-20} cm^2 for O_2. A solar irradiance value of 3×10^{11} cm^{-2} s^{-1}, corresponding to solar minimum conditions, has been adopted. A secondary ion source due to the absorption of ultraviolet light in the 102.7-111.8 nm spectral range by the metastable $^1\Delta_g$ oxygen molecules has been determined according to Paulsen et al. [1972]. Hard X rays (0.2-1 nm) are usually of minor importance except during high solar activity periods. The values adopted for the solar irradiance are similar to that reproduced in Brasseur [1982]. The absorption and ionization cross sections are taken from Banks and Kockarts [1973].

TABLE 1. Adopted Values of the Ionization Rate at 65° Latitude due to Relativistic Electrons Precipitation

Altitude	Ionization Rate cm^{-3} s^{-1}
50	0.1
55	0.2
60	0.4
65	0.9
70	1.6
75	2.7
80	4.3
85	6.3
90	8.9
95	11.7
100	14.1

The ionization Q due to galactic cosmic rays, which becomes dominant in the lower part of the D region and in the stratosphere, has been calculated using the parameterization formula suggested by Heaps [1978], namely,

$$Q = [A + B \sin^4 \Lambda]\, n(M)$$

where $A = 1.74 \times 10^{-18}$ s^{-1}, and $B = 2.84 \times 10^{-17}$ s^{-1}, and 1.96×10^{-17} s^{-1}, respectively, for low and high solar activity conditions. In this expression, Λ is the geomagnetic latitude, which has been assimilated to the geographic latitude, and n(M) is the total atmospheric concentration.

The effect of relativistic electrons precipitating from the magnetosphere in the

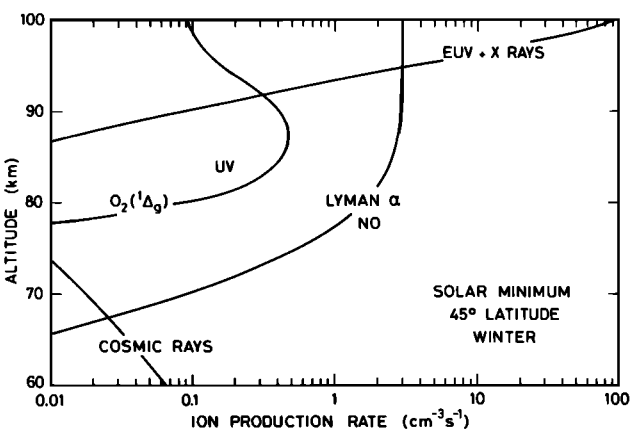

Fig. 5. Vertical distribution of the various contributions to the ion production rate calculated at 45° latitude in summer for a quiet sun including ionization of atmospheric gases by EUV and X rays, photoionization of nitric oxide by Lyman α, ionization of $O_2(^1\Delta g)$ by UV light, and the effect of the cosmic rays.

TABLE 2. Reactions of Positive ions with Neutrals.

Reaction	Rate Constant $cm^3\ s^{-1}$
$O_2^+ + O_2 \rightarrow O_4^+$	$2.6 \times 10^{-30} (300/T)^{3.2}$ n(M)
$O_2^+ + NO \rightarrow NO + O_2$	4.4×10^{-10}
$O_2^+ + N \rightarrow NO^+ + O$	1.2×10^{-10}
$O_4^+ + O \rightarrow O_2^+ + O_3$	3.0×10^{-10}
$O_4^+ + H_2O \rightarrow O_2^+ . H_2O + O_2$	1.5×10^{-9}
$O_2^+ . H_2O + H_2O \rightarrow H_3O^+ . OH + O_2$	1.0×10^{-9}
$O_2^+ . H_2O + H_2 \rightarrow H_3O^+ + OH + O_2$	$\leq 2.0 \times 10^{-11}$
$H^+(H_2O) + H_2O \rightarrow H^+(H_2O)_2$	$3.4 \times 10^{-27} (300/T)^{4.0}$ n(M)
$H^+(H_2O)_2 + M \rightarrow H^+(H_2O) + H_2O + M$	$9.6 \times 10^{11}\ T^{-5}\ e^{-17100/T}$
$H^+(H_2O)_2 + H_2O \rightarrow H^+(H_2O)_3$	$2.3 \times 10^{-27} (300/T)^{4.0}$ n(M)
$H^+(H_2O)_3 + M \rightarrow H^+(H_2O)_2 + H_2O + M$	$1.95 \times 10^{11}\ T^{-5}\ e^{-11000/T}$
$H^+ . (H_2O)_3 + H_2O \rightarrow H^+ . (H_2O)_4$	$2.4 \times 10^{-27} (300/T)^{4.0}$ n(M)
$H^+ . (H_2O)_4 + M \rightarrow H^+ . (H_2O)_3 + H_2O + M$	$1.36 \times 10^{11}\ T^{-5}\ e^{-8360/T}$
$H_3O^+ . OH + H_2O \rightarrow H^+(H_2O)_2 + OH$	1.4×10^{-9}
$NO^+ + H_2O \rightarrow NO^+ . H_2O$	$1.8 \times 10^{-28} (308/T)^{4.7}$ n(M)
$NO^+ + CO_2 \rightarrow NO^+ . CO_2$	$7.0 \times 10^{-30} (300/T)^{3.0}$ n(M)
$NO^+ + N_2 \rightarrow NO^+ . N_2$	$2.0 \times 10^{-31} (300/T)^{4.4}$ n(M)
$NO^+ . CO_2 + M \rightarrow NO^+ + CO_2 + M$	$3.1 \times 10^{4}\ T^{-4}\ e^{-4590/T}$
$NO^+ . CO_2 + H_2O \rightarrow NO^+ . H_2O + CO_2$	1.0×10^{-9}
$NO^+ . N_2 + M \rightarrow NO^+ + N_2 + M$	$1.5 \times 10^{6}\ T^{-5.4}\ e^{-2450/T}$
$NO^+ . N_2 + CO_2 \rightarrow NO^+ . CO_2 + N_2$	1.0×10^{-9}
$NO^+ . H_2O + H_2O \rightarrow NO^+ . (H_2O)_2$	$1.0 \times 10^{-27} (308/T)^{4.7}$ n(M)
$NO^+ . H_2O + CO_2 \rightarrow NO^+ . H_2O . CO_2$	$7.0 \times 10^{-30} (300/T)^{3.0}$ n(M)
$NO^+ . H_2O + N_2 \rightarrow NO^+ . H_2O . N_2$	$2.0 \times 10^{-31} (300/T)^{4.4}$ n(M)
$NO^+ . (H_2O)_2 + H_2O \rightarrow NO^+ . (H_2O)_3$	$1.0 \times 10^{-27} (308/T)^{4.7}$ n(M)
$NO^+ . (H_2O)_2 + CO_2 \rightarrow NO^+ . (H_2O)_2 . CO_2$	$7.0 \times 10^{-30} (300/T)^{3.0}$ n(M)
$NO^+ . (H_2O)_2 + N_2 \rightarrow NO^+ . (H_2O)_2 . N_2$	$2.0 \times 10^{-31} (300/T)^{4.4}$ n(M)
$NO^+ . (H_2O)_3 + H_2O \rightarrow H^+ . (H_2O)_3 + HNO$	7.0×10^{-11}
$NO^+ . H_2O . CO_2 + M \rightarrow NO^+ . H_2O + CO_2 + M$	$3.1 \times 10^{4}\ T^{-4}\ e^{-4025/T}$
$NO^+ . H_2O . CO_2 + H_2O \rightarrow NO^+ . (H_2O)_2 + CO_2$	1.0×10^{-9}
$NO^+ . H_2O . N_2 + M \rightarrow NO^+ . H_2O + N_2 + M$	$1.5 \times 10^{6}\ T^{-5.4}\ e^{-2150/T}$
$NO^+ . (H_2O)_2 . CO_2 + M \rightarrow NO^+ . (H_2O)_2 + CO_2 + M$	$3.1 \times 10^{4}\ T^{-4}\ e^{-3335/T}$
$NO^+ . (H_2O)_2 . CO_2 + H_2O \rightarrow NO^+ (H_2O)_3 + CO_2$	1.0×10^{-9}
$NO^+ . H_2O . N_2 + CO_2 \rightarrow NO^+ . H_2O . CO_2 + N_2$	1.0×10^{-9}
$NO^+ . (H_2O)_2 . N_2 + M \rightarrow NO^+ . (H_2O)_2 + N_2 + M$	$1.5 \times 10^{6}\ T^{-5.4}\ e^{-1800/T}$
$NO^+ . (H_2O)_2 . N_2 + CO_2 \rightarrow NO^+ . (H_2O)_2 . CO_2 + N_2$	1.0×10^{-9}

n(M) = atmospheric density (cm^{-3})
T = temperature (K)

subauroral belts (65° ± 5° of latitude) has been considered [Thorne, 1977] by adopting an average ionization rate, as given in Table 1. The strength and the occurrence of such electron precipitation processes is not well known. The numbers which are adopted should thus be considered as working values to qualitatively assess the effects of this ionization source. Figure 5 shows the various contributions of the ionization rate calculated at 45° latitude in winter for solar minimum conditions.

The ion chemistry of the D region has been discussed in several papers (see, e.g., Nicolet [1945]; Nicolet and Aikin [1960]; Reid [1970, 1976]; Thomas [1974]; Mitra [1981]; etc.), and a series of models, mostly one-dimensional, have been constructed [Sechrist, 1972; Hunt, 1973. Rowe et al., 1974; Thomas, 1976; Reid, 1976; Dymek, 1980; Wisemberg and Kockarts, 1980, Sears et al., 1981, Forbes, 1981; Torkar and Friedrich, 1983; André, 1983, etc.] to explain, for example, the mass spectrometer observations of positive and negative ions [e.g., Narcisi and Bailey, 1965; Goldberg and Blumle, 1970; Goldberg and Aikin, 1971; Arnold 1980; Kopp and Herrmann, 1984, etc.]. A model study of the D region ion chemistry was also presented by Solomon et al. [1982b] with the purpose of determining whether the observable data regarding ions could be used to infer information regarding the neutral composition.

Observations clearly indicate, as expected from the early theory [Nicolet, 1945], that NO^+ is the dominant ion above 75-85 km altitude but that water cluster ions are the most abundant below this altitude level [Narcisi and Bailey, 1965]. The presence of these latter ions has been explained by Fehsenfeld and Ferguson [1969] and by Reid [1977], who have shown that both O_2^+ and NO^+ primary ions lead to the formation of $H^+(H_2O)_n$ clusters. The chemical scheme suggested by Thomas [1974] and Reid [1976] has been adopted in this paper, with the rate constants as given in Table 2. Most of these rate constants are taken from the compilation by Albritton [1978]. Some laboratory measurements might be uncertain and require further discussion. For example, the formation of H_3O^+ from $O_2^+.H_2O$ with H_2O is now believed to be endothermic [Fehsenfeld and Ferguson, 1969; Kopp and Herrmann, 1984]. However, since the oxonium ion distribution is controlled mainly by thermochemical equilibrium of hydration, the final result should not be influenced by the accuracy of the branching ratio of this reaction. The destruction of the ions occurs either by electron recombination, with a rate of the order of 4×10^{-6} cm^3 s^{-1} or by negative ion recombination with a corresponding rate close to 6×10^{-8} cm^3 s^{-1}.

Negative ions are produced by electron attachment processes and subsequent reactions, which are given in Table 3. The primary negative ion O_2^- is transformed through a chain of reactions which is not yet completely understood, although it has been studied extensively in recent years (see, e.g., Ferguson [1979]).

This chain ultimately leads to stable ions such as NO_3^-, CO_3^- or HCO_3^-. Since the ratio between the NO_3^- and CO_3^- concentration is a function of the amount of nitric oxide, it should be highly dependent on the dynamical conditions in the atmosphere and should decrease considerably during the night when NO is converted into NO_2. Observations made during solar eclipses show [André, 1983] low concentrations of NO_3^- and high CO_3^- amounts. Hydrates of the NO_3^- and CO_3^- ions are also probably formed and should even be prevalent in the nighttime ionosphere [Keesee et al. , 1979]. Since these hydrates are not explicitly calculated in the present model, the calculated values of NO_3^- or CO_3^- concentrations should include that of the corresponding hydrates. Furthermore, in the vicinity of the stratopause and in the stratosphere, NO_3^- cores can also be clustered with HNO_3 molecules. Photodetachment of electrons and photodissociation of molecular ions have also been considered, with daytime values of the corresponding rates, as indicated in Table 3. These values, also used in the model of Wisemberg and Kockarts [1980], are based on the measurements of photodestruction cross sections by Smith et al. [1978], and Lee and Smith [1979]. These laboratory data, which are reported as upper limits, lead to destruction rates which are highly uncertain, since, for example, the branching ratio between photodetachment and photodissociation is not well known. Therefore large uncertainty should be associated with the calculated electron concentration below about 70 km. Adopted recombination rates of positive and negative ions are given in Table 4.

Cl^- ions have not yet been introduced in the model but, to a first approximation, their concentration can be obtained by considering the following reactions

$$(k_A)\ ;\ O_2^- + HCl \rightarrow Cl^- + HO_2 \quad (1.6\times10^{-9}\ cm^3\ s^{-1})$$

$$(k_B)\ ;\ O^- + HCl \rightarrow Cl^- + OH \quad (2.0\times10^{-9}\ cm^3\ s^{-1})$$

$$(k_C)\ ;\ Cl^- + H \rightarrow HCl + e^- \quad (9.6\times10^{-10}\ cm^3\ s^{-1})$$

so that

$$n(Cl^-) = \frac{k_A\, n(O_2^-) + k_B\, n(O^-)}{k_c\, n(H)}\, n(HCl) \qquad (1)$$

In order to calculate the ion concentration a balance equation is associated to each positive and negative ion, taking into account all reactions appearing in Tables 2-4. Two distinct matrixes, corresponding to the positive and to the negative charges, respectively, are solved in sequence, making use of the neutrality equation

$$n(e) + n(Y^-) = n(Y^+) = (1 + \lambda)\, n(e) \qquad (2)$$

In this expression, n(e), $n(Y^-)$, and $n(Y^+)$ are the electron concentration and the total concentration of negative and positive ions, respectively. The λ parameter is the ratio between the negative ion and the electron concentration. An iteration is performed with an initial distribution of the electron concentration and of the λ parameter. Only a few iterations are required to achieve convergence and fulfill the electroneutrality condition.

When adding all equations referring to positive or to negative charges, one obtains the following expression, assuming that the values of

TABLE 3a. Reactions Between Negative Ions and Neutrals and Corresponding Rate Constant

Reaction	Rate Constant $cm^3\ s^{-1}$	
$O^- + O_3 \rightarrow O_3^- + O$	8.0×10^{-10}	
$O^- + CO_2 \rightarrow CO_3^-$	3.1×10^{-28}	n(M)
$O^- + NO_2 \rightarrow NO_2^- + O$	1.0×10^{-9}	
$O^- + H_2 \rightarrow OH^- + H$	3.2×10^{-11}	
$O^- + CH_4 \rightarrow OH^- + CH_3$	1.0×10^{-10}	
$O^- + O_2(^1\Delta g) \rightarrow e + O_3$	3.0×10^{-10}	
$O^- + H_2 \rightarrow e + H_2O$	6.0×10^{-10}	
$O^- + O \rightarrow e + O_2$	1.9×10^{-10}	
$O^- + NO \rightarrow e + NO_2$	2.8×10^{-10}	
$O_2^- + O \rightarrow O^- + O_2$	1.5×10^{-10}	
$O_2^- + O_3 \rightarrow O_3^- + O_2$	7.8×10^{-10}	
$O_2^- + NO_2 \rightarrow NO_2^- + O_2$	7.0×10^{-10}	
$O_2^- + CO_2 \rightarrow CO_4^-$	4.7×10^{-29}	n(M)
$O_2^- + O_2 \rightarrow O_4^-$	3.4×10^{-31}	n(M)
$O_2^- + O_2(^1\Delta g) \rightarrow e + 2O_2$	2.0×10^{-10}	
$O_2^- + O \rightarrow e + O_3$	1.5×10^{-10}	
$O_2^- + H \rightarrow e + HO_2$	1.4×10^{-9}	
$O_2^- + H_2O \rightarrow O_2^-.H_2O$	2.2×10^{-28}	n(M)
$O_2^-.H_2O + CO_2 \rightarrow CO_4^- + H_2O$	5.8×10^{-10}	
$O_2^-.H_2O + NO \rightarrow NO_3^- + H_2O$	2.0×10^{-10}	
$O_3^- + O \rightarrow O_2^- + O_2$	2.5×10^{-10}	
$O_3^- + H \rightarrow OH^- + O_2$	8.4×10^{-10}	
$O_3^- + CO_2 \rightarrow CO_3^- + O_2$	5.5×10^{-10}	
$O_3^- + NO_2 \rightarrow NO_3^- + O_2$	2.8×10^{-10}	
$O_3^- + NO \rightarrow NO_3^- + O$	4.5×10^{-12}	
$CO_3^- + O \rightarrow O_2^- + CO_2$	1.1×10^{-10}	
$CO_3^- + H \rightarrow OH^- + CO_2$	1.7×10^{-10}	
$CO_3^- + NO \rightarrow NO_2^- + CO_2$	1.0×10^{-11}	
$CO_3^- + NO_2 \rightarrow NO_3^- + CO_2$	2.0×10^{-10}	
$NO_2^- + O_3 \rightarrow NO_3^- + O_2$	1.2×10^{-10}	
$NO_2^- + NO_2 \rightarrow NO_3^- + NO$	2.0×10^{-13}	
$NO_2^- + H \rightarrow OH^- + NO$	3.0×10^{-10}	
$OH^- + NO_2 \rightarrow NO_2^- + OH$	1.1×10^{-9}	
$OH^- + O_3 \rightarrow O_3^- + OH$	9.0×10^{-10}	
$OH^- + CO_2 \rightarrow HCO_3^-$	7.6×10^{-28}	n(M)
$OH^- + H \rightarrow e + H_2O$	1.4×10^{-9}	
$OH^- + O \rightarrow e + HO_2$	2.0×10^{-10}	

Table 3a. (continued)

Reaction	Rate Constant $cm^3\ s^{-1}$
$O_4^- + O \rightarrow O_3^- + O_2$	4.0×10^{-10}
$O_4^- + CO_2 \rightarrow CO_4^- + O_2$	4.3×10^{-10}
$O_4^- + NO \rightarrow NO_3^- + O_2$	2.5×10^{-10}
$O_4^- + H_2O \rightarrow O_2^-(H_2O) + O_2$	1.0×10^{-10}
$CO_4^- + O_3 \rightarrow O_3^- + CO_2 + O_2$	1.3×10^{-10}
$CO_4^- + O \rightarrow CO_3^- + O_2$	1.4×10^{-10}
$CO_4^- + H \rightarrow CO_3^- + OH$	2.2×10^{-10}
$CO_4^- + NO \rightarrow NO_3^- + CO_2$	4.8×10^{-11}
$CO_4^- + H_2O \rightarrow O_2^-.H_2O + CO_2$	2.5×10^{-10}

n(M) = atmospheric density (cm^{-3})

the electron clusters and ion-ion recombination coefficients are the same for all ions,

$$q(\text{ion-pair}) = [\alpha(NO^+)\, n(NO^+) + \alpha(O_2^+)\, n(O_2^+) + \alpha_c\, n(\text{clusters}^+)]n(e) + \alpha_i\, n(Y^+)\, n(Y^-) \quad (3)$$

where q is the ion pair production, $\alpha(NO^+)$, $\alpha(O_2^+)$, and α_c are the ion-electron recombination coefficients for NO^+, O_2^+, and the cluster ions, and α_i is the ion-ion recombination coefficient. Assuming now that $\alpha(NO^+) \simeq \alpha(O_2^+) \equiv \alpha_D$, and introducing the f^+ parameter defined as

$$f^+ = \frac{n(\text{clusters}^+)}{n(NO^+) + n(O_2^+)} \quad (4)$$

and using

$$\lambda = \frac{n(Y^-)}{n(e)} \quad (5)$$

TABLE 3b. Photodetachment and Photodissociation Rates

Reaction	Rate Constant seconds
$O^- + h\nu \rightarrow e + O$	1.4
$O_2^- + h\nu \rightarrow e + O_2$	0.38
$OH^- + h\nu \rightarrow e + OH$	1.1
$NO_2^- + h\nu \rightarrow e + NO_2$	8.0×10^{-4}
$CO_3^- + h\nu \rightarrow O^- + CO_2$	0.15
$O_3^- + h\nu \rightarrow O^- + O_2$	0.47
$CO_4^- + h\nu \rightarrow O_2^- + CO_2$	6.2×10^{-3}
$O_4^- + h\nu \rightarrow O_2^- + O_2$	0.24

TABLE 4. Recombination Rates

Reaction	Rate Constant $cm^3\ s^{-1}$
$X^- + Y^+ \rightarrow$ neutrals	6.0×10^{-8}
$e + O_2^+ \rightarrow$ neutrals	$1.9 \times 10^{-7}\ (300/T)^{0.5}$
$e + NO^+ \rightarrow$ neutrals	$2.3 \times 10^{-7}\ (300/T)^{0.5}$
$e + Y^+ \rightarrow$ neutrals	4.0×10^{-6}

the electron production rate is given by

$$q(\text{electrons}) = \frac{q(\text{ion-pair})}{1 + \lambda} \qquad (6)$$

and the effective electron recombination coefficient by

$$\alpha_{eff}(\text{electrons}) = \frac{\alpha_D + f^+ \alpha_c}{1 + f^+} + \lambda\, \alpha_i \qquad (7)$$

These parameters, namely, λ, q(ion-pair), and α_{eff} (electrons), which define the main characteristics of the electron layer, are dependent on the state of the neutral atmosphere, in particular on the dynamical and photochemical processes.

Results of the Ion Model and Discussion

The number of free electric charges which are present in the atmosphere depends on the strength of the total ionization rate. This latter value, which is represented as a function of the altitude and the latitude in Figure 6, varies considerably with time and space. Above 90 km (E region) the production rate of ion pairs is driven directly by the action of EUV radiation on the major gases (O_2, N_2). Its maximum value is thus located at the subsolar point. Below 85 km (D region) the ionization rate is proportional to the local concentration of nitric oxide, which is significantly larger in the winter hemisphere than in the region where the irradiation is the most intense. As already shown by Solomon et al. [1982b], a real asymmetry between hemispheres therefore appears in the ionization rate distribution (see also Figure 7). The largest contribution to the ion production rate at 95 km clearly follows the variation of cos χ_{noon}, where χ_{noon} is the solar zenith angle at noon, while at 85 km and below the latitudinal distribution of nitric oxide and consequently transport processes controls the state of the ionosphere (see also Solomon et al. [1982b]). It should be noted from Figure 7 that the contribution of the $O_2(^1\Delta_g)$ ionization becomes relatively large in summer when the NO concentration is small. The action of cosmic rays appears to be significant (Figure 6) below 65 km altitude, where the ionization increases with increasing latitude. The effects of particle precipitation and in particular the contribution of the relativistic electrons (REP) can be seen in narrow belts located around 65° latitude.

The morphology of the ionosphere is related not only to the meridional distribution of the ion production rate, whose 24-hour averaged value is represented in Fig. 6, but also to the effective recombination coefficient α_{eff}. Above 75 km the electric neutrality is achieved by a balance between positive ions and electrons. Below this altitude level, electrons get pro-

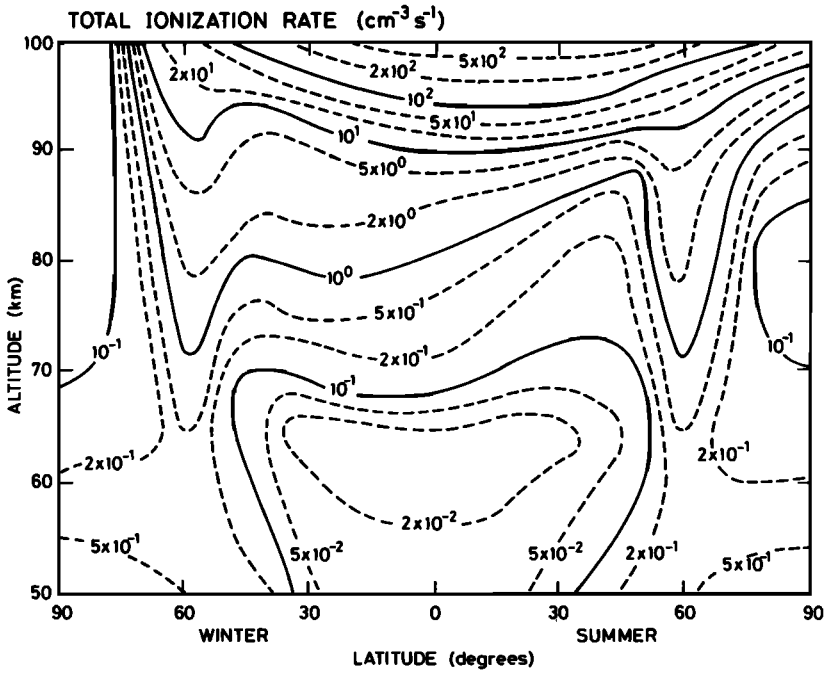

Fig. 6. Meridional distribution of the total ion production rate (24-hour average) calculated in the model and used for determination of the concentration of the individual ions.

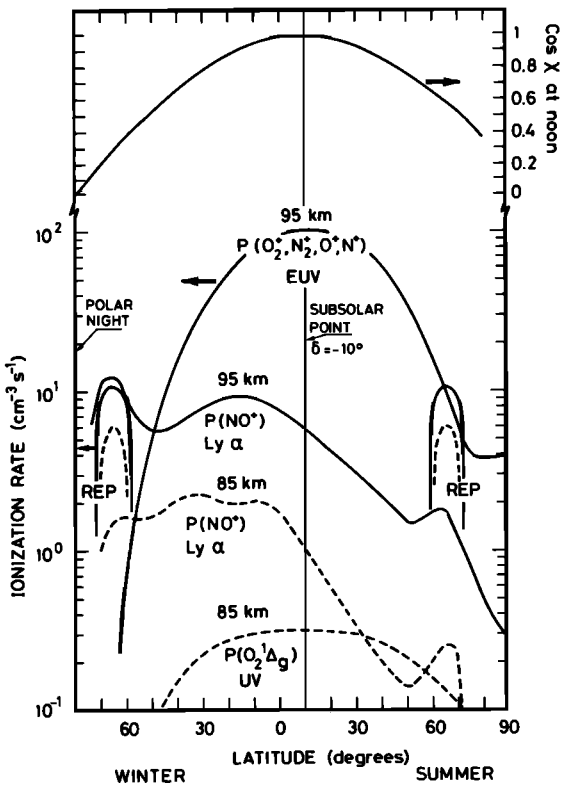

Fig. 7. Latitudinal distribution of the various contributions to the ionization rate at 95 and 85 km, respectively.

gressively attached to neutral particles, leading to the presence of the negative ions. The effect is described by the λ parameter (see expression (5)). The concentration of the individual ions depends on the rate constant values, which are associated with the many reactions occurring between ions and neutral species, and consequently, on the local temperature.

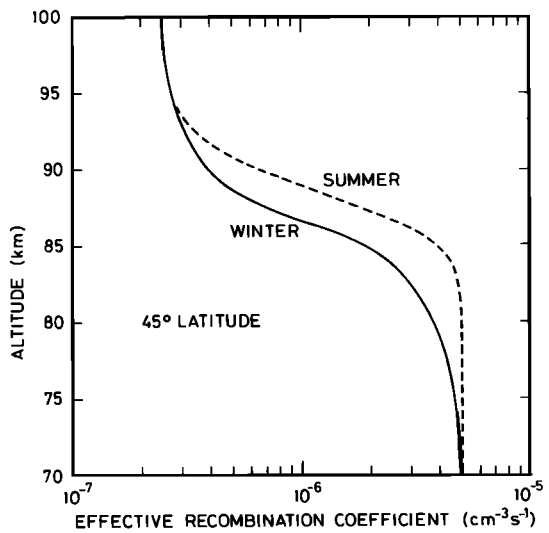

Fig. 8. Effective recombination coefficient of electrons at 45° latitude for winter and summer conditions, respectively.

Electrons

Electrons play a specific role in the ionosphere because of their ability to interact with radio waves. Although their concentration in the model is obtained, as for any other ion, from the global equations system, it is useful for analysis of the result to consider the simple equation

$$n(e) = \left[\frac{q(\text{ion-pair})}{(1+\lambda)\ \alpha_{eff}} \right]^{1/2} \qquad (8)$$

which indicates that at high altitude ($\lambda \ll 1$) the electron concentration depends only on two parameters. The first parameter, the ion production rate, has been discussed previously. The second factor, α_{eff}, depends on the composition (see expression (7)) and more specifically on the f^+ parameter, that is, on the relative amount of cluster ions. In the E region above 90 km, where NO^+ and O_2^+ are totally dominant ($f^+ \ll 1$), the effective recombination coefficient α_{eff} is close to $\alpha_D \simeq 2.5 \times 10^{-7}$ cm^3 s^{-1}. Below 75 km, however, the cluster ions are the most abundant ($f^+ \gg 1$)

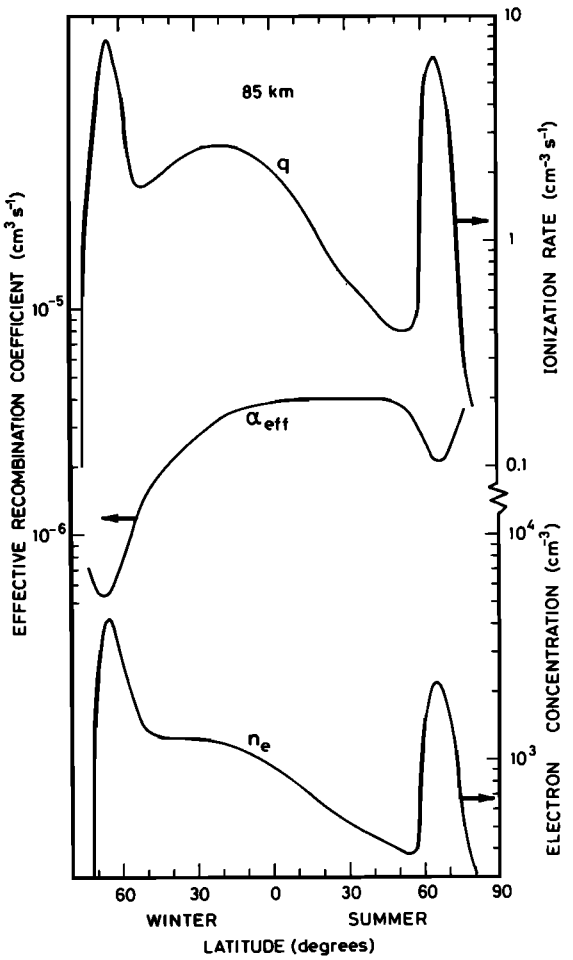

Fig. 9. Latitudinal distribution at 85 km altitude of the ionization rate, the effective recombination coefficient, and the electron concentration.

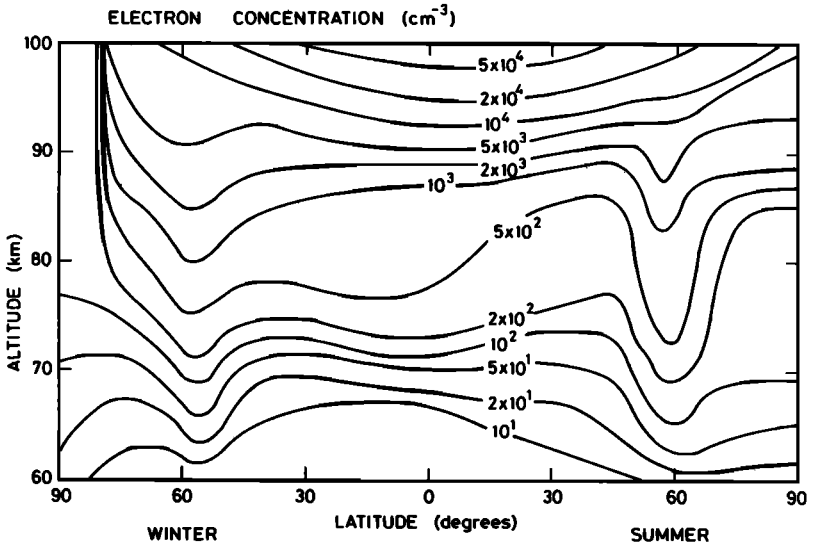

Fig. 10. Meridional distribution of the electron concentration between 60 and 100 km altitude in a winter and summer hemisphere.

and $\alpha_{eff} \simeq \alpha_D = 5 \times 10^{-6}$ cm^3 s^{-1}. Between these two regions, α_{eff} is variable with altitude and, since its value depends on the ion composition and on the temperature, his height variation changes with the local conditions and differs from one season to another. In winter, when the average mesopause temperature is high, the clusters break up rather easily, leading to small values of the f^+ parameter and of the α_{eff} coefficient. In summer, when the average mesopause temperature is low, the situation is reversed (see Figure 8). This effect has been invoked to explain at least partly the short-time and seasonal variation of the electron concentration and in some cases the winter anomalous radio wave absorption in the D region. It is now believed, however [Offermann et al., 1982; Solomon et al., 1982b], that even if the temperature effect cannot be entirely rejected, the essential cause of the winter anomaly is the sporadic intrusions of nitric oxide from the thermosphere due to enhanced vertical transport activity and to a subsequent increase in the D region ionization rate. For illustration purposes, Figure 9 shows the latitudinal distribution at the mesopause of the ionization rate, the recombination coefficient, and the electron concentration. It can be seen that both the formation and the destruction rates of electrons vary with latitude so that the electron concentration is definitely higher in the winter hemisphere. The precipitation of energetic particles in the auroral belts decreases the local value of the f^+ factor and consequently the value of the α_{eff} coefficient. In other words the precipitation of particles (REP, aurorae) enhances the relative amount of O_2^+ and NO^+ versus the cluster concentration. This can easily be explained from the expression which describes the balance between cluster formation and destruction [Kopp and Hermann, 1984], namely,

$$f^+ = \frac{n(clust^+)}{n(NO^+) + n(O_2^+)} = \frac{k(T)\ \rho^n}{\alpha_{eff}\ n(e) + g(O)} \qquad (9)$$

ρ being the total air density, g(O) a function of the atomic oxygen concentration, k(T) the rate constant of cluster formation which varies from about T^{-3} to T^{-5} [Reid, 1976], and n an exponent whose value lies between 2 and 4. The large number of electrons in the auroral belts reduces f^+. The expression above also shows the importance of the atomic oxygen concentration in the ionospheric morphology. As pointed out by Kopp and Herrman [1984], a larger O concentration in the winter hemisphere due to enhanced downward transport would help to reduce f^+ and consequently to increase the electron concentration during this season. Sporadic ozone enhancement in the lower thermosphere as observed by the SME satellite [Thomas et al., 1983] and probably related to vertical transport of atomic oxygen, could reinforce anomalous radio wave absorption event.

Figure 10 represents the meridional distribu-

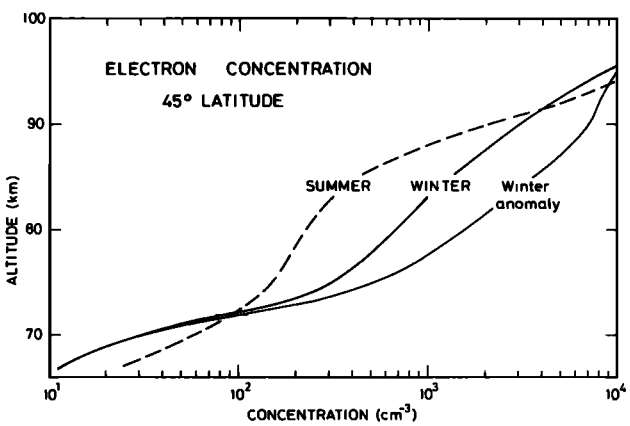

Fig. 11. Vertical distribution between 65 and 100 km at 45° latitude of the electron concentration for summer and winter conditions. The curve labeled "winter anomaly" has been obtained by doubling the nitric oxide injection at 100 km altitude in the winter hemisphere.

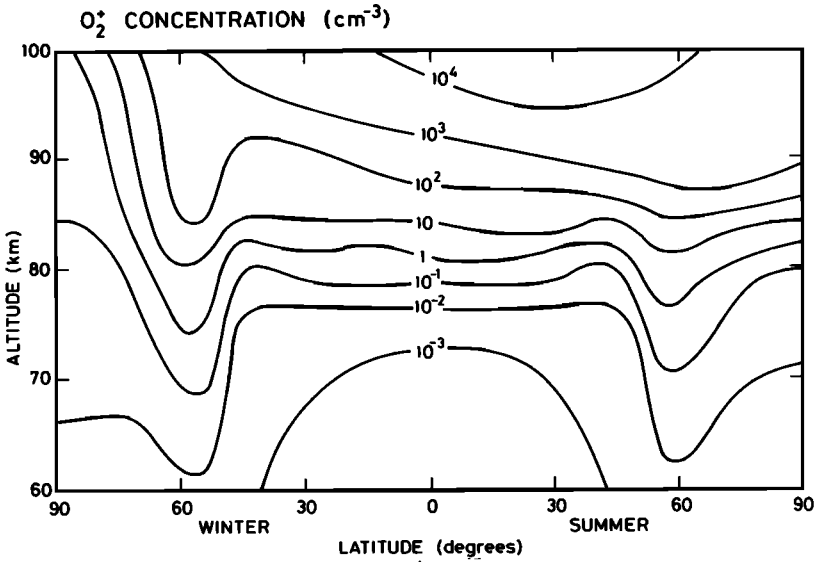

Fig. 12a. Meridional distribution of the O_2^+ concentration between 60 and 100 km for a winter and a summer hemisphere.

tion of the electron concentration which is obtained for a 24-hour averaged illumination. Again, the different physical processes, which have been discussed previously, are reflected in Figure 10. The relation between the electrons concentration and solar zenith angle is evident above 90 km. In the region between 70 and 90 km the effect of NO appears through a hemispherical asymmetry. Below 70 km the action of the cosmic rays can be inferred from the concentration contours. The specific conditions in the auroral zones are also apparent.

As also suggested from the observations, the model (Figure 10) provides an electron concentration value at 80-85 km which is a factor of 3 to 4 higher in winter than in summer. In order to simulate a sporadic winter anomaly event qualitatively, the NO_x intrusion from the thermosphere at 100 km has been arbitrarily multiplied by 5 in winter at all latitudes in order to evaluate the response of the ionosphere to such events when they occur at different locations. At 45° latitude, for example, the nitric oxide concentration is enhanced by a factor of 4.5 at 85 km, 3.4 at 75 km, and 2.8 at 65 km. The corresponding change in the electron concentration is quite significant, as shown in Figure 11. The resulting enhancement in the radio wave absorption at 45° latitude is close to a factor of 3, in good agreement with the calculation of Solomon et al. [1982b] but slightly larger than the observed value of the regular winter anomaly (a factor of 2 in Lindau, Federal Republic of Germany; see Schwentek [1971]). Thus the model, which represents a seasonal averaged situation, probably reflects a mixture between the regular and irregular anomalous enhancement in radio wave absorption.

Positive Ions

The meridional distribution of the primary ions O_2^+ and NO^+ is represented in Figures 12a and b. In both cases,, the different ionization

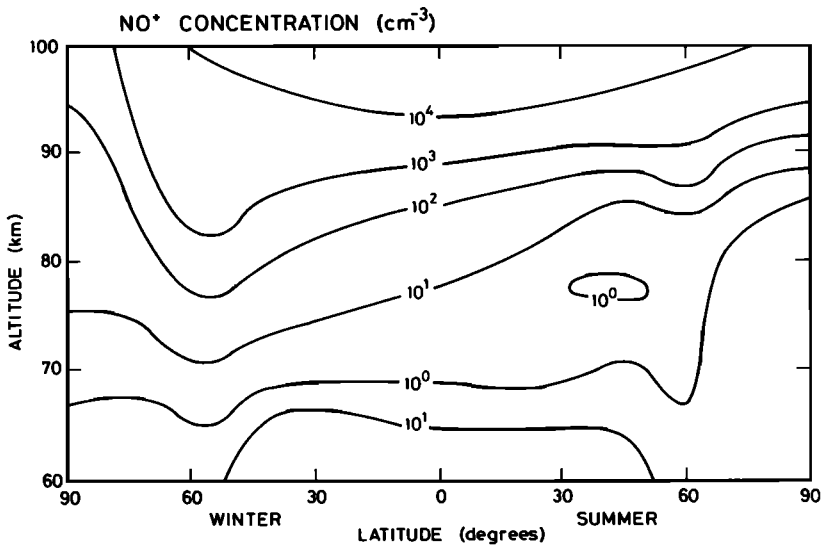

Fig. 12b. Same as Figure 12a but for NO .

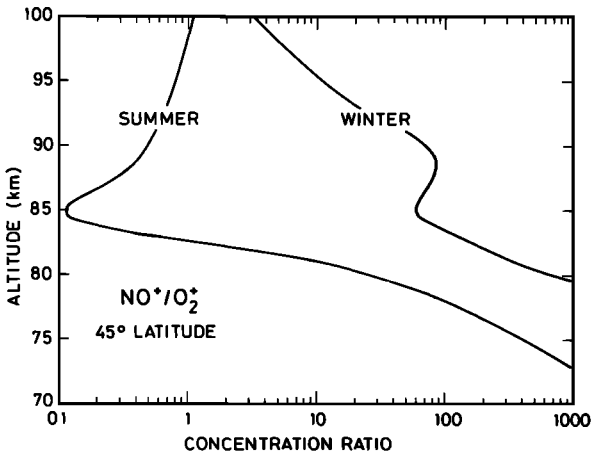

Fig. 13. Vertical profile of the concentration ratio of NO^+ to O_2^+ at 45° latitude. Note the differences between winter and summer conditions.

regimes are again reflected in the morphology of the ion concentration. However, in the D region, O_2^+ is the most abundant in the summer hemisphere, while the NO^+ concentration reaches its maximum in winter. This seasonal difference has to be attributed to the charge exchange reaction between O_2^+ and NO^+, whose rate is directly proportional to the nitric oxide concentration. The ratio between NO^+ and O_2^+ is thus highly variable with latitude and season, as suggested by Figure 13 and is directly controlled by the mesospheric dynamics.

The water clusters $H^+(H_2O)_n$ are produced either from O_2^+ or from NO^+. They become the most abundant ions below 75-85 km, depending on the geophysical conditions. Figure 14 shows the amount of cluster ions relative to the total number of positive ions, as calculated from the model at 60° latitude (winter and summer). Data reported by Kopp and Herrmann [1984] during a quiet day, a winter anomaly event, and an aurora either at Wallops Island or at Kiruna are also indicated. The theoretical results show that the transition height ($f^+ = 1$), which is located at 85 km in summer, decreases to about 81.5 km in winter (normal day) and to 78 km during a simulated winter anomaly event. A decrease of this transition altitude is also derived from the observations, but the absolute height seems on the average somewhat lower than the calculated values.

The concentration of the most abundant positive ions versus altitude at mid-latitude is plotted in Figures 15a-15d for winter and summer conditions. The winter profiles correspond essentially to a rather wet and warm hemisphere with a large amount of nitric oxide, while the summer profiles are characteristic of a rather dry and cold hemisphere with a very small amount of NO_x. The model indicates that the most abundant ions below 80 km are $H^+(H_2O)_3$ and $H^+(H_2O)_{\geq 4}$ (essentially n = 4). The characteristic "flat top" of these distributions is observed in all mass spectrometer observations and is explained by the number of successive reactions which are involved in producing these clusters, so that their concentration is proportional to the atmospheric density raised by a large power n (see expression (9)). Moreover, the large electron and atomic oxygen concentration at high altitudes contributes to the existence of this "flat top".

Above 80 km in winter, NO^+ becomes the major single ion, but appreciable concentrations of its hydrates are also present up to 90 km. In summer, as a result of the low temperature in the vicinity of the mesopause, thermal breakup of NO^+ clusters is weaker, and the concentration of $NO^+(H_2O)$ becomes larger than that of the single NO^+ ion. Moreover, the characteristic "flat top" of the water clusters lies somewhat higher despite the low water vapor concentration. Figure 16 shows the meridional distribution of one of these water clusters, namely, $H^+(H_2O)_3$. Most of the latitudinal variability is related to the spatial variation in the cosmic rays intensity and in the temperature.

The relative amount of each individual proton hydrate can be derived to a first approximation from the relation

$$\frac{n[H^+(H_2O)_n]}{n[H^+(H_2O)_{n-1}]} = \frac{k_f\, n(M)\, n(H_2O)}{k_r\, n(M) + \alpha_c n(e)} \qquad (10)$$

where k_f and k_r are the rate constants for the forward and the reverse reaction path of

$$H^+(H_2O)_{n-1} + H_2O + M \rightarrow H^+(H_2O)_n + M \qquad (11)$$

respectively, and α_c is the recombination coefficient of $H^+(H_2O)_n$ with electrons. Equation (10) will thus be a function of the temperature, particularly at low altitudes, where it is proportional to the equilibrium constant of (11). At high altitudes (above about 85 km) the recombination becomes more important than the thermal breakup and the ratio between the nth and (n-1)th cluster becomes sensitive, through the electron concentration, to particle precipitation

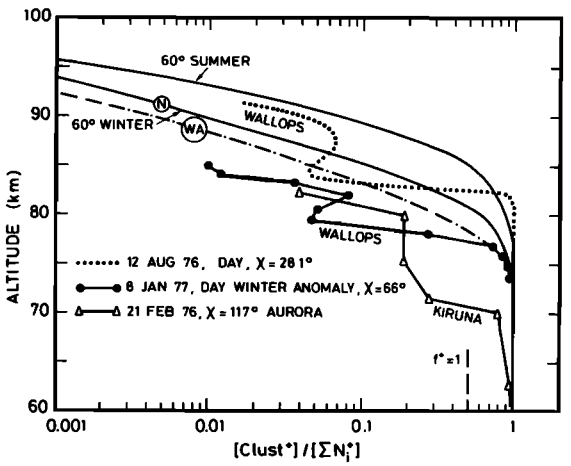

Fig. 14. Calculated and observed distribution of the ratio between the clusters (proton hydrates) and the total ion concentrations at high latitude. The curve labeled N refers to a normal winter day and the curve labeled WA to an anomalous day (assuming a doubled intrusion of NO at 100 km). The observed distributions are from Kopp and Herrmann [1984].

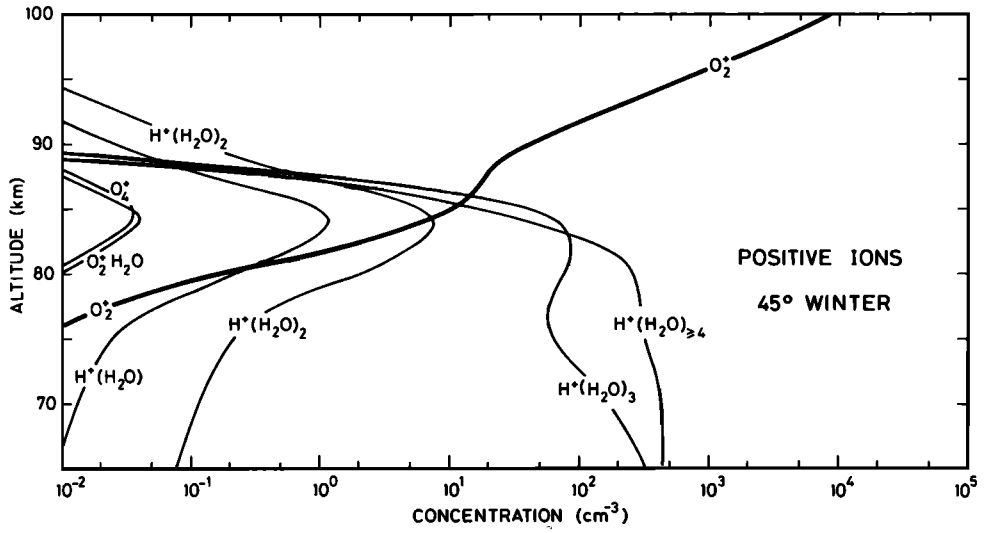

Fig. 15a. Vertical distribution of selected positive ions at 45° for winter.

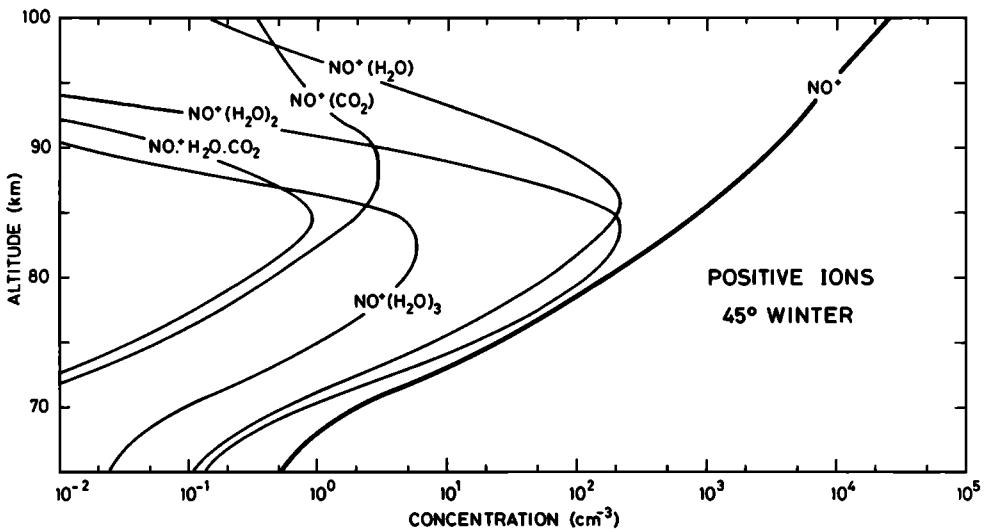

Fig. 15b. Vertical distribution of selected positive ions at 45° for winter conditions.

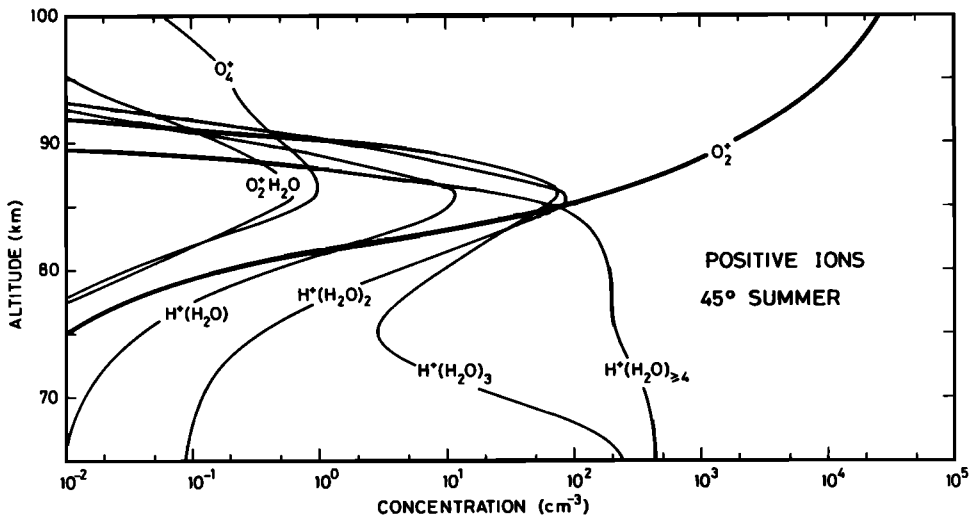

Fig. 15c. Vertical distribution of selected positive ions at 45° for summer conditions.

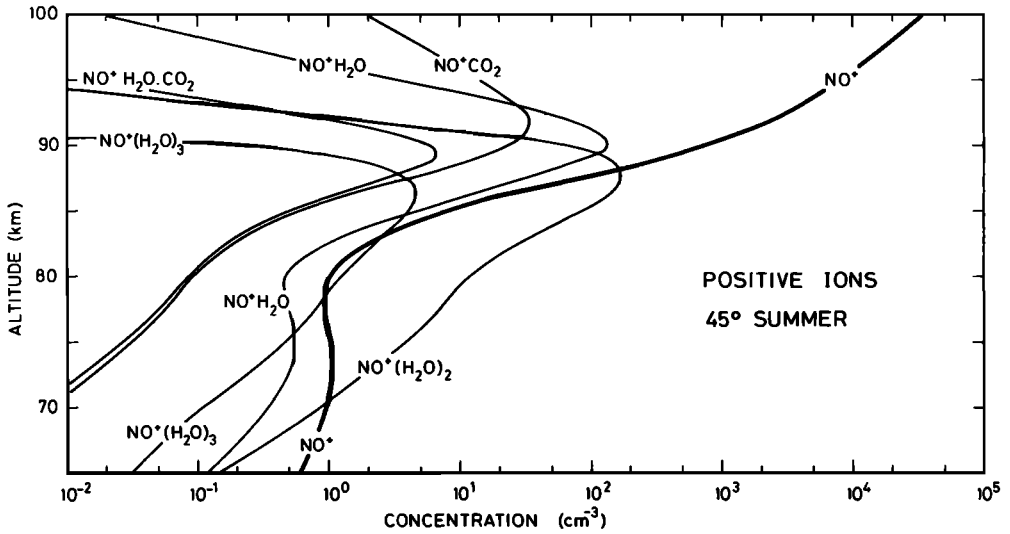

Fig. 15d. Vertical distribution of selected positive ions at 45° for summer conditions.

during aurorae,polar cap absorption events, REP, etc. Moreover, since NO^+ is a primary ion to the third hydrate $H^+(H_2O)_3$ and not to the first and second hydrates, the relative amount of each proton hydrate to the total cluster ions will be dependent on the NO amount and consequently will vary with altitude, latitude, season, and geophysical conditions (Figure 17).

The comparison of the calculated ion distributions with sporadic observations is thus quite difficult. Theoretical values are obtained using average model input for parameters which fluctuate considerably in the real world (temperature, water vapor, nitric oxide, particle precipitation, etc.) Moreover, destruction of several ions, such as the high water clusters which breakup easily, occurs in some experiments during the sampling process, which makes the comparison hazardous. Therefore the theoretical results, although they reproduce the general features of the observed distributions (see, e.g., Kopp et al., [1978]; Kopp and Hermann [1984]), sometimes exhibit considerable differences, which are also found when comparing several individual observed profiles.

Negative Ions

The λ ratio (Figure 18) becomes larger than unity below 72 to 75 km, so that the negative ions contribute significantly to the negative charges in the atmosphere below 75 km. As indicated previously, the primary negative ion O_2^- is converted into a stable final ion NO_3^- if nitric oxide is present. During the night (or during a solar eclipse), when NO is converted into NO_2, the reaction chain is shorter and the final ion is CO_3^-. Most of these stable ions can be clustered with other molecules, in particular, water vapor. Figures 19a and 19b show the

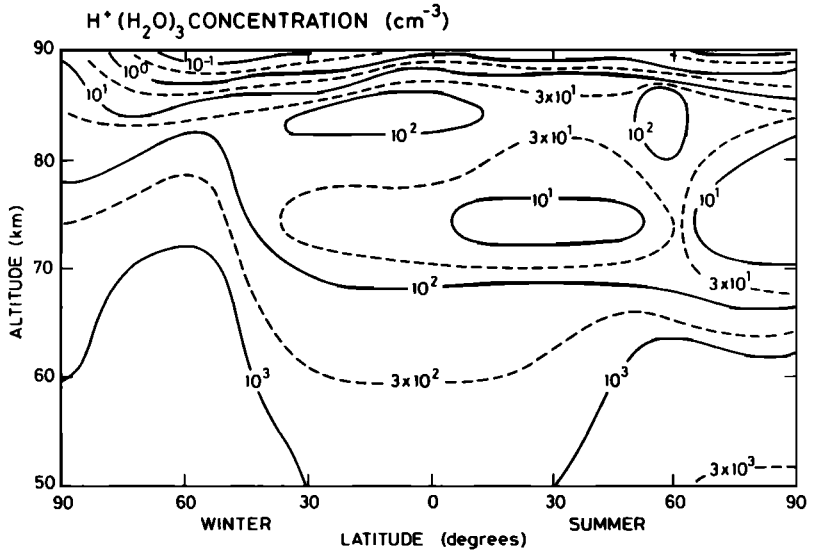

Fig. 16. Meridional distribution of the $H^+(H_2O)_3$ concentration calculated between 50 and 90 km altitude.

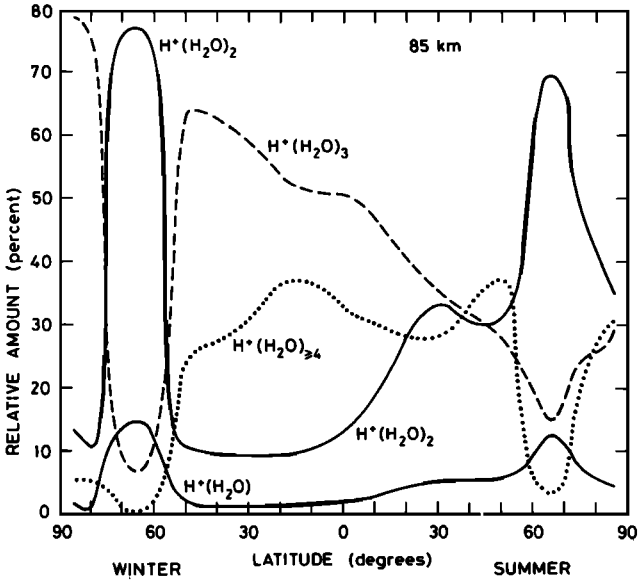

Fig. 17. Relative amount of individual cluster ions as a function of latitude.

calculated vertical distribution of the most abundant negative ions at 45° latitude (winter and summer). The ratio between the NO_3^- and the CO_3^- concentration appears to be larger, at least above 60 km, in winter than in summer, when NO is the most abundant. Again, the profile of these species is directly controlled by the thermospheric and mesospheric dynamics and the geophysical conditions through the nitric oxide distribution. The HCO_3^- ion becomes dominant above 70 km, especially in summer, when the amount of NO_3^- is reduced. Its concentration is proportional to the atomic hydrogen concentration, which is considerably reduced during the night in the mesosphere. Cl^- atoms should also appear in rather large quantities after sunset, since, as indicated by (1), the loss of this ion no longer occurs during the night. The two-dimensional calculated distributions of NO_3^- and CO_3^- are shown in Figures 20a and 20b. Only a very few observations of negative ions in the D region are available. These are not consistent with the profiles predicted from theoretical models based on laboratory measurements of reaction rates.

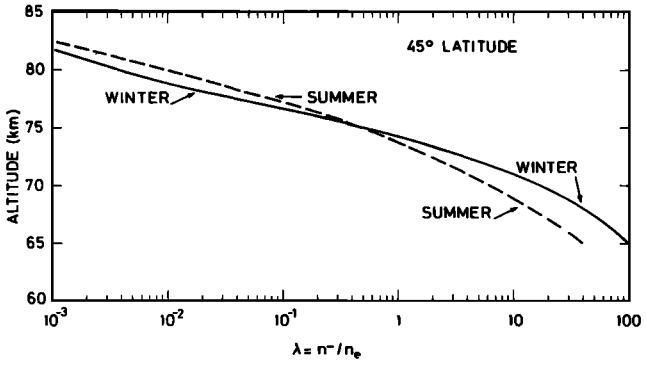

Fig. 18. Vertical distribution of the ratio λ between negative ion and electron concentrations. Summer and winter conditions.

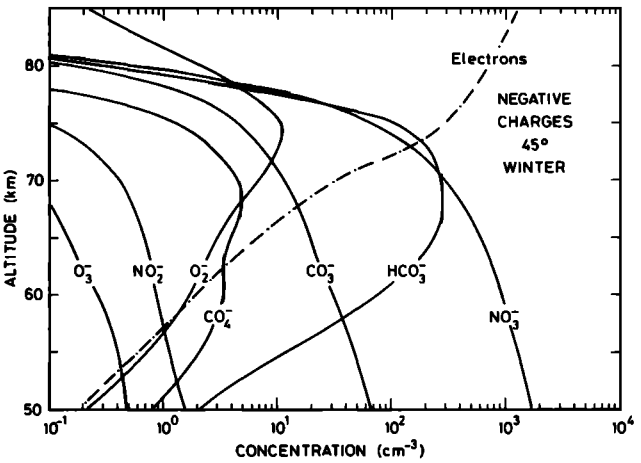

Fig. 19a. Vertical distribution of negative ion concentration at 45° latitude in winter.

Laboratory work as well as in situ observations are thus required.

Ionospheric Response to the 11-Year Solar Cycle

Systematic measurements of the solar irradiance in the ultraviolet have shown that a substantial variation occurs, at least below 200 nm, with a period of 27 days (rotation period of the sun; Rottman [1983]) and also with a period of 11 years [Heath and Thekaekara, 1977; Mount et al., 1980; Hinteregger, 1981]. The magnitude of the 11-year modulation is, however, difficult to establish because of the possible differences in the calibration of the various instruments used over a specific solar cycle or the instrument drift associated with satellite experiments.

Several models of the solar variability as a function of wavelength have been used to assess the chemical or thermal response of the middle atmosphere to the 11-year cycle [Heath and Thekaekara, 1977; Penner and Chang, 1978, 1980; Callis and Neally, 1978a, b; Callis et al., 1979; Natarajan et al. 1981; Brasseur and Simon, 1981; De Baets et al., 1981; Lean et al., 1982; Garcia et al., 1984]. The model used in this work, which

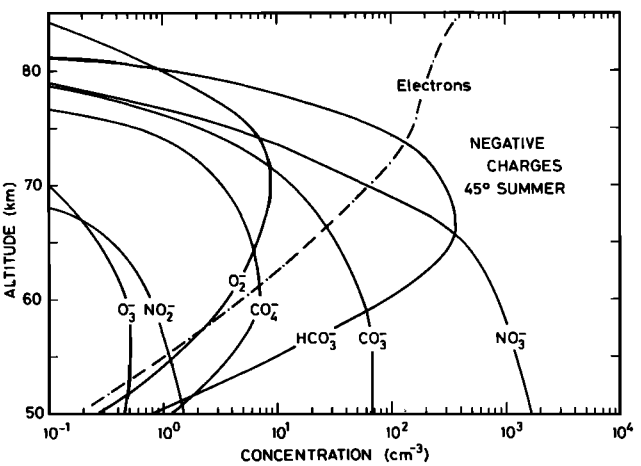

Fig. 19b. Vertical distribution of negative ion concentration at 45° latitude in summer.

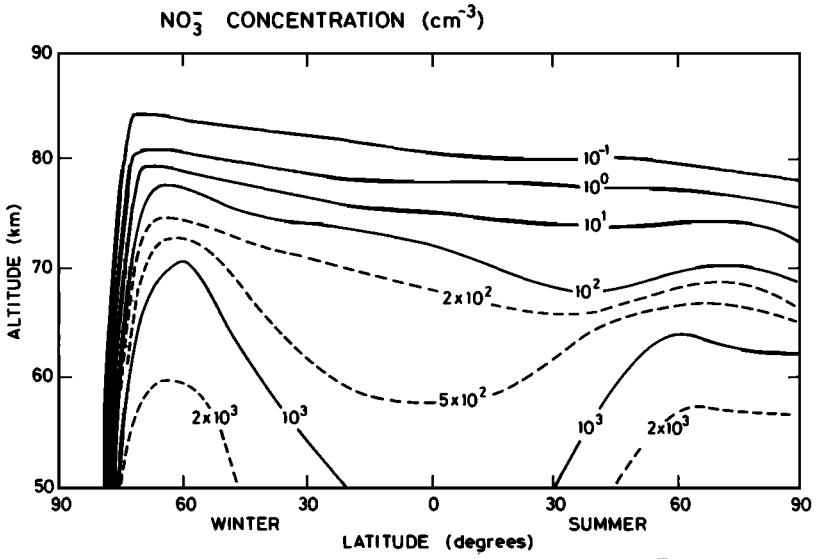

Fig. 20a. Meridional distribution of the concentration of NO_3^- between 50 and 90 km altitude.

is similar to that of Brasseur et al. [1983], is based on the analysis by Hinteregger [1981], as shown by Figure 21. This model assumes a variability of about a factor of 2 at wavelengths shorter than 150 nm, including Lyman α. At higher wavelengths the change in the irradiance decreases to reach less than 20% in and above the region of the Schumann-Runge bands. Above the aluminium edge in the solar spectrum at 208 nm the irradiance is assumed to remain unchanged, since its origin is photospheric.

Although the suggested variability over most of the spectrum is smaller than in previous models [Heath and Thekaekara, 1977; Penner and Chang, 1978; Natarajan et al., 1981], it should still be considered as an upper limit below 200 nm if one refers to the analysis by Nicolet [1983], leading to a variability of 11 ± 4% near 180 nm, and by Bossy [1983], stating a 40% variation at Lyman α. The change in the solar irradiance above 208 nm is difficult to measure, since the real variation is smaller than the accuracy in the instruments. The effects of this part of the spectrum occur mostly in the stratosphere, that is, below the lower boundary of the model, and the zero variability which is adopted in the model is without consequence on the calculated values above the stratopause.

The solar variability in the EUV and X ray portion of the spectrum is specified in the model according to Brasseur [1982]. These values are based on data published by Banks and Kockarts [1973] and Nicolet and Bossy [1981].

Finally, since the state of the magnetosphere and in particular its ability to shield the atmosphere from particle precipitation increases with solar activity, a variation in the cosmic rays intensity has been introduced according to the parameterization by Heaps [1978]. The ionization due to cosmic rays, which becomes the

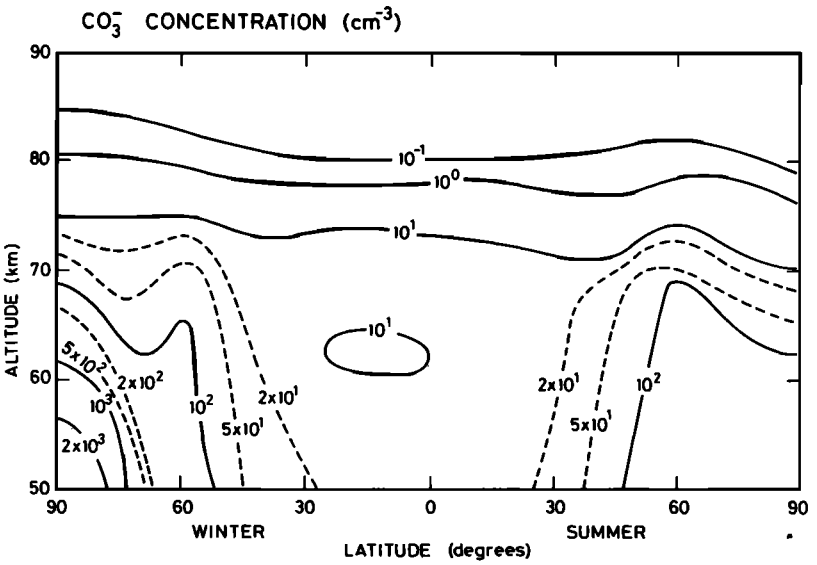

Fig. 20b. Meridional distribution of the concentration of CO_3^- between 50 and 90 km altitude.

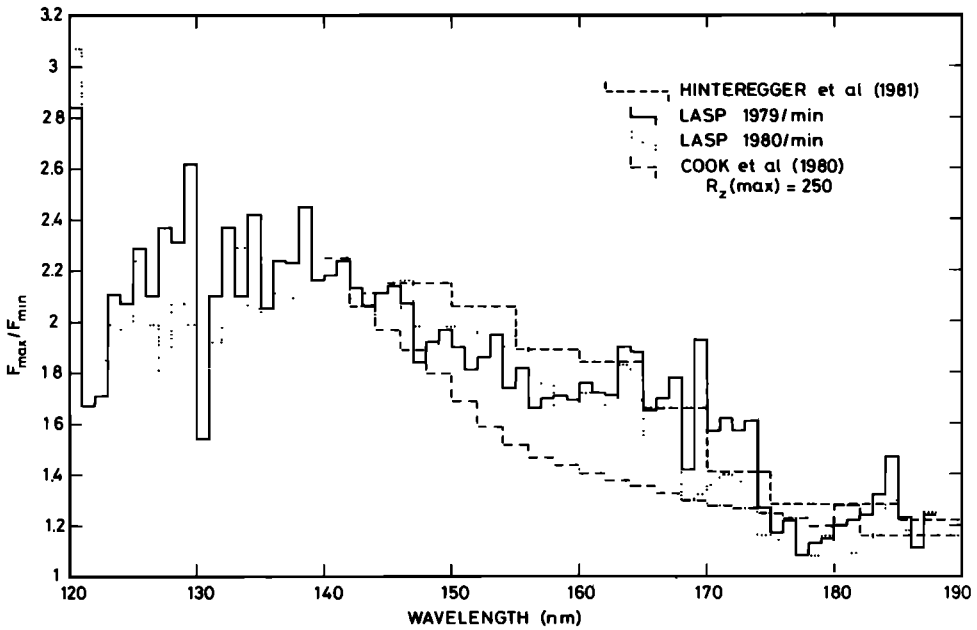

Fig. 21. Solar irradiance variation from 120 to 190 nm between maximum and minimum values during the 11-year solar cycle. Variability derived from observational data by Hinteregger [1981] and from rocket observations. LASP refers to data from the Laboratory for Atmospheric and Space Physics, University of Colorado, Boulder, Co., published in Mount et al., [1980], Rottman [1981] and Mount and Rottman [1981]. Model by Cook et al. [1980].

dominant ionization process below 70 km, decreases with enhanced solar activity.

Among the atmospheric responses to an enhanced solar irradiance, the increase in the thermospheric production of nitric oxide plays an important role. Such an effect should be particularly noticeable in the auroral zones where considerable amounts of NO_x are produced. These effects occur essentially above the upper limit of our model and will be reflected through a variable upper boundary condition. As in the previous paper by Brasseur et al. [1983], the downward flux of NO_x at 100 km is assumed to change by a factor of 2 during a solar cycle. A similar variation of the integrated nitric oxide production in the thermosphere has been adopted by Garcia et al. [1984] at 116 km and is in good agreement with the value suggested by Roble and Emery [1983].

The present model of the relation between the atmospheric composition and the 11-year solar cycle is purely photochemical and keeps the thermal and dynamical parameters unchanged. This should not considerably alter the calculated variations in the chemical composition, since as shown by Garcia et al. [1984] and Geller and Alpert [1980], the change in the averaged wind and the planetary wave structure and consequently in the transport of trace species is rather small. Moreover, the predicted temperature change becomes considerable only in the upper mesosphere and thermosphere, where the thermal feedback on the chemistry is expected to be smaller than near the stratopause.

The response of the ionosphere to solar activity is quantitatively estimated by adopting, for the changes in the neutral species, the results of Brasseur et al. [1983]. From this study the variation in the nitric oxide concentration from solar minimum to solar maximum appears to be quite different in winter and summer, respectively. In the first case the increase of NO_x with solar activity is due to the higher injection of odd nitrogen from the thermosphere. A variation of about 60%, 40% and 10% is calculated for the NO_x concentration at 80 km, 70 km, and at the stratopause, respectively. In summer the effect of the enhanced thermospheric NO_x production does not propagate below 85 km, since the vertical transport is weak in this hemisphere. Below the mesopause, a reduction in the concentration appears (- 10% at 70-80 km and 40° latitude) and is due to the enhancement of the NO photodissociation coefficient, which is estimated to be of the order of 20%.

The modulation of the water vapor mixing ratio with solar cycle is also dependent on the season. In the winter hemisphere where transport dominates, the change is considerably smaller (- 15% at 80 km and 60° latitude) than in the summer hemisphere (-38% at 80 km and 60° latitude) where the destruction of the H_2O molecule is due to its photodissociation, mainly by Lyman α. Our quantitative estimate of the water vapor variability is in good agreement with Garcia et al. [1984]. Garcia et al., however, show less seasonal dependence of the water vapor response than the present calculation.

The change in the odd oxygen content which is adopted in the present study is different from the values calculated previously by Brasseur et al. [1983], since it has been determined by doubling the O_x concentration at 100 km in order to account for the larger photodissociation rate of O_2 when the solar irradiance increases (a

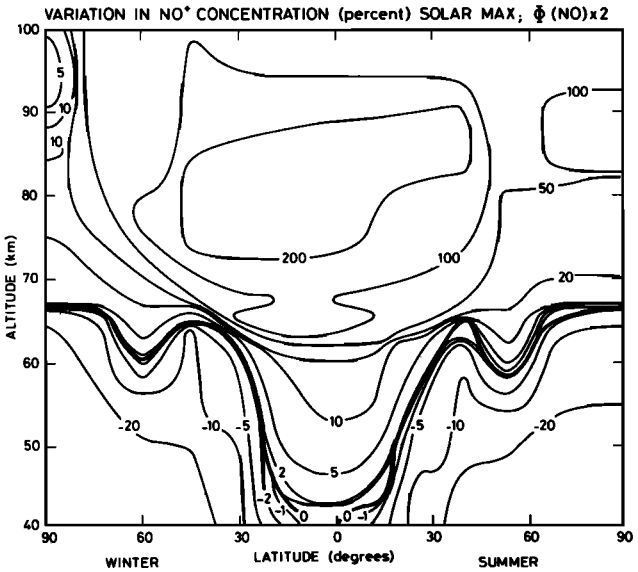

Fig. 22a. Relative percent variation in the concentration of NO^+ from solar minumum to maximum conditions (11-year solar cycle).

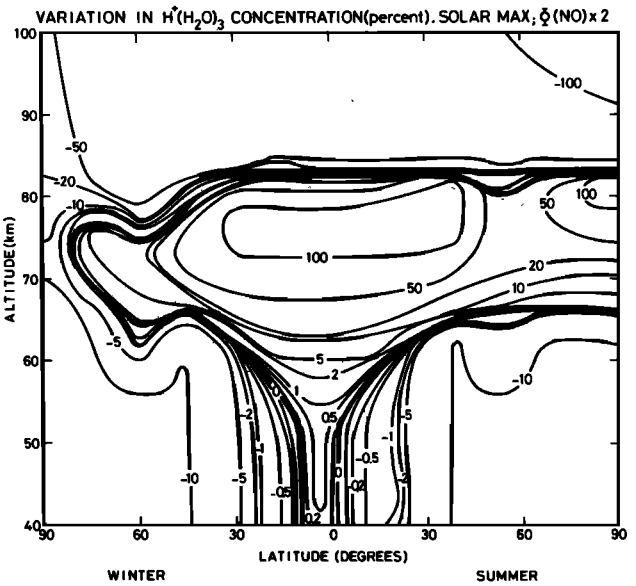

Fig. 22c. Same as Figure 22a but for $H^+(H_2O)_3$.

variation of a factor of 2 is expected over the solar cycle in the spectral region of the Schumann-Runge continuum where most of the photolysis of O_2 takes place). The resulting variation of O_x is predicted to be of the order of 70% at 90 km, that is, a factor of 2.5 and 1.5 larger than the values derived by Allen et al. [1984] and Garcia et al. [1984], respectively. At 80 km the change in O_x is predicted to be of the order of 20-40%, that is, a factor of 2-4 larger than the values calculated by Allen et al. [1984] (10%) and a factor of about 2 smaller than the prediction by Garcia et al. [1984] (60-80%).

In the lower thermosphere the changes in the atomic oxygen and ozone concentration are dominated by the modulation of the photodissociation rate of molecular oxygen, while in the mesosphere the variation in both the odd hydrogen concentration and in the O_2 photodissociation rate plays a role. The relative importance of these two processes varies with the average optical depth, that is, with latitude and season, so that the largest increase in the odd oxygen concentration occurs in the summer hemisphere. Close to the stratopause the predicted O_x variation is small, in agreement with Allen et al. [1984] and Garcia et al. [1984].

The long-term changes in the ionization rate have also been discussed by Brasseur et al. [1983]. In the D region these variations are due simultaneously to the enhancement of the NO concentration in relation with the higher odd nitrogen injection from the thermosphere, and to the increase in the strength of the Lyman α line. In the E region the main ion source is due to the action of the EUV radiation on the major gases N_2 and O_2. The effect of X rays can be neglected in the D and E regions during quiet sun conditions but becomes significant when solar flares occur. The relative variation in the concentration of selected ions is shown in Fig. 22a-22d.

The maximum change for the primary ions NO^+

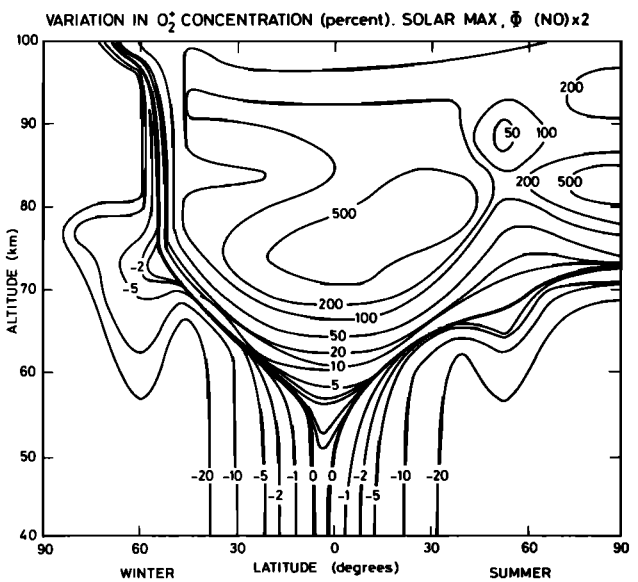

Fig. 22b. Same as Figure 22a but for O_2^+.

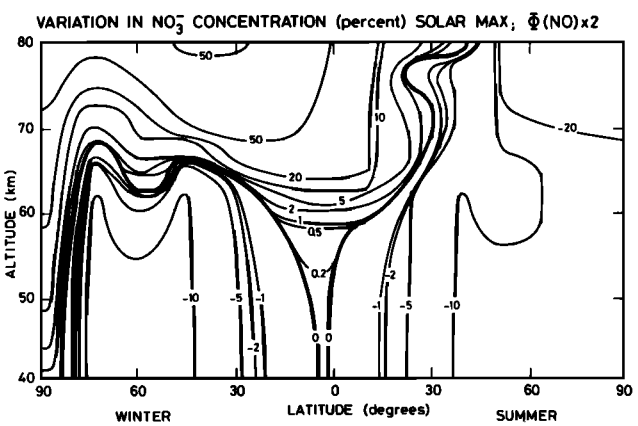

Fig. 22d. Same as Figure 22a but for NO_3^-.

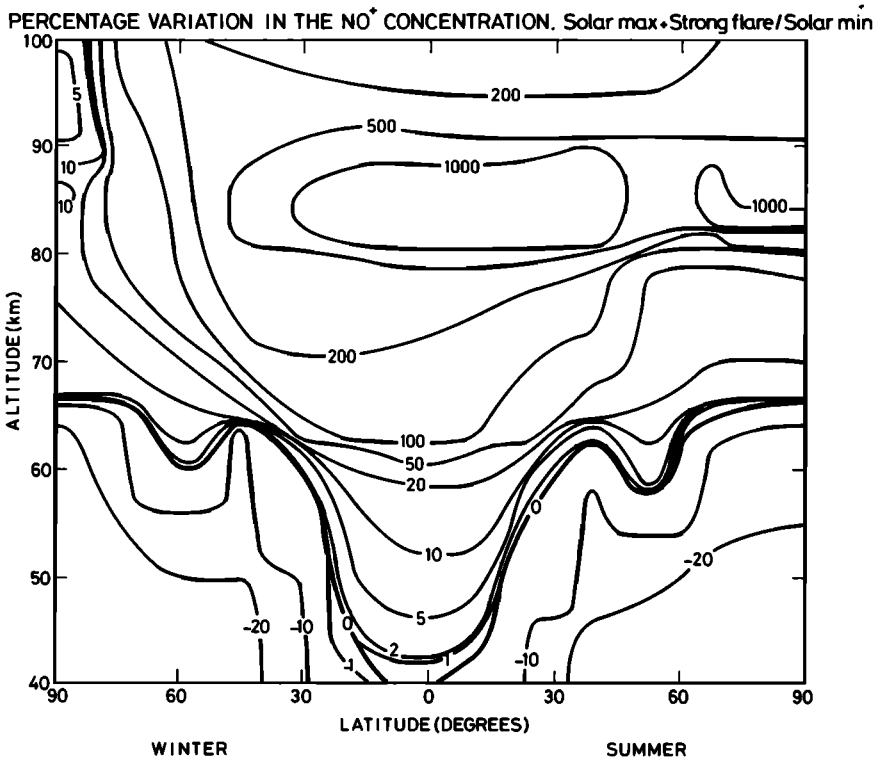

Fig. 23. Relative percent change in the concentration of NO^+ due to the effect of a strong solar flare (see text for details).

and O_2^+ (Figures 22a and 22b) occurs in the vicinity of the mesopause in the equatorial region. The predicted change of NO^+ in the D region in summer is essentially due to the enhancement of the ionizing radiation and in winter to the increase in the NO concentration. The variation in the O_2^+ concentration in the D and E regions is also driven by the change in the nitric oxide amount. Indeed, when NO is considerably enhanced, a larger part of O_2^+ is converted into NO^+ by reaction

$$O_2^+ + NO \rightarrow NO^+ + O_2$$

Such an effect occurs particularly in the winter hemisphere and explains why the O_2^+ variation becomes negative above 60° latitude. Below 65 km, especially at high latitude, the variability in the ion concentration is driven by the change in the cosmic rays, which is out of phase with the solar activity. A negative change, up to about 10 to 20%, is predicted for most ions below 65 km altitude.

In the D region, $H^+(H_2O)_3$, whose production results from several clustering reactions subsequent to the NO^+ formation, exhibits a similar meridional distribution of the response to solar activity (see Figure 22c). In the E region, however, where the formation of $H^+(H_2O)_n$ results from the hydration of O_2^+, the variation becomes negative because of the decrease in the water vapor concentration and the increase in the amount of atomic oxygen. Atomic oxygen reduces the efficiency of the O_2^+ clustering chain by enhancing the decomposition of the O_4^+ ion (see Table 3a.) This effect does not play any considerable role, since at these heights the concentration of proton hydrates becomes considerably smaller than that of the primary ions. Figure 22d shows the long-term variability of one of the most abundant negative ions, NO_3^-. Again, the effect of cosmic rays appears below 65 km, while at higher altitudes, the change is essentially due to the variation in the NO concentration.

Finally, in order to qualitatively predict the effect of a strong flare on the ionic composition, the strength of the X rays below 1 nm has been increased by a factor of 100 compared to solar maximum conditions (or by a factor of 10^5 compared to completely quiet conditions) - [see Banks and Kockarts, 1973, Table 7.5]. Since the largest flares generally occur during the period of high solar activity, solar maximum conditions have been assumed for all other parameters. The predicted concentrations have been compared to solar minimum values. Figure 23 shows, for example, that the NO^+ concentration is enhanced by a factor of 1000 in the vicinity of the mesopause, leading to dramatic changes in all ionospheric conditions above 65 km. Similar variations for the electron concentration are calculated, leading to considerable perturbations in the radio propagation.

To conclude this section, it should be noted that the solar emission at short wavelength varies rather randomly with time along a solar cycle and that the predicted changes in the species concentration do not reflect a particular situation but provide a qualitative explanation for observed variations. The simulation of a real case requires the introduction in the model of an accurate spectral distribution of the actual solar irradiance.

Conclusions

Model calculations show that the behavior of neutral and ionic species exhibits a large latitudinal dependence due to dynamical processes, temperature variations, and the distribution of solar input and high-energy particle precipitation. In particular, the physical and chemical conditions are significantly modified with the actual season.

In winter, when photochemistry is less active and vertical mixing becomes very strong, nitric oxide is transported from the thermosphere to the stratosphere, such that the two layers are strongly coupled: the amount of NO at the stratopause varies with the strength of the odd nitrogen production by ionospheric processes above 100 km and with the intensity of vertical exhanges in the lower thermosphere and in the mesosphere. Other species involved in ionospheric chemistry, such as atomic oxygen and water vapor, are also dependent on the strength of the dynamics.

In summer, nitric oxide produced in the thermosphere is destroyed in the mesosphere by photodissociation and recombination. This loss process is facilitated by the low temperature at the mesopause during the summer. Atomic oxygen is expected to remain at higher altitudes than in winter, due to the upward circulation and the relatively low vertical exhange coefficient. The mixing ratio of water vapor decreases significantly above 70 km, as a result of its photodissociation.

The concentration of positive and negative ions is directly dependent upon the distribution of neutral long-lived species. Therefore although the lifetime of ions below 100 km is relatively short, the D region appears to be dynamically controlled, especially in winter.

Sporadic effects, such as anomalous absorption of radio waves in the D region, seem to be related to the variability in the nitric oxide injection from the thermosphere when the dynamics exhibit strong variability. The relative amount of several ions, such as the proton hydrates, appears also to be very sensitive to the changes in local temperature and in the intensity of particle precipitation.

Finally, noticeable changes in the meridional distribution of neutral and ionic species should be attributed to variability in the solar output, in relation, for example, to the 11-year solar cycle.

Systematic observations of trace species in the mesosphere and in the thermosphere should lead to a better understanding of the various coupling mechanisms occurring in these layers, and in particular should reveal the importance of dynamical processes on the behavior of chemical constituents.

Acknowledgments. We wish to thank S. Solomon, E. Arijs, D. Offermann, E. Kopp and M. Dymek for stimulating discussions and interesting suggestions during the preparation of this paper.

References

Abdu, M. A., and I. S. Batista, Nitric oxide height distribution in the lower ionosphere from rocket ion composition results over a southern temperature latitude station, J. Geophys. Res., 84, 5267, 1979.

Allen, M., J. I. Lunine, and Y. L. Yung, The vertical distribution of ozone in the mesosphere and lower thermosphere, J. Geophys. Res., 89, 4841, 1984.

Allen, M., Y. L. Yung, and J. W. Waters, Vertical transport and photochemistry in the terrestrial mesosphere and lower thermosphere (50-120 km), J. Geophys. Res., 86, 3617, 1981.

Albritton, D. L., Ion-neutral reaction rate constants measured in flow reactors through 1977, At. Data Nucl. Data Tables, 22, 1, 1978.

André, L., Negative ion composition for different conditions in the mesosphere, Proceedings of the sixth ESA Symposium on Rocket and Balloon Programmes Eur. Space Agency Spec. Publ.(ESA SP-183), 103, 1983.

Arnold, F., The middle atmosphere ionized component, Proceedings of the ESA Symposium on Rocket and Balloon Programmes Eur. Space Agency Publ. (ESA SP-152), 479, 1980.

Baker, K. D., A. F. Nagy, R. O. Olsen and E. S. Oran, Measurement of nitric oxide distribution in the mid-latitude mesosphere, J. Geophys. Res., 82, 3281, 1977.

Banks, P. M. and G. Kockarts, Aeronomy, part A, Academic, Orlando, Fla 1973.

Beran, D. and W. Bangert, Trace constituents in the mesosphere and lower thermosphere during winter anomaly events, J. Atmos. Terr. Phys., 41, 1091, 1979.

Bossy, L., Solar indices and solar UV irradiances, Planet. Space Sci., 31, 977, 1983.

Brasseur, G. Physique et Chimie de l'Atmosphère Moyenne, Masson, Paris, 1982.

Brasseur G., Coupling between the thermospshere and the stratosphere : the role of nitric oxide, MAP Handbook, vol. 10 edited by J. Taubenheim, pp. 116-121, University of Illinois, Urbana, 1984.

Brasseur G, and A. Chatel, Modelling of stratospheric ions : A first attempt, Ann. Geophys., Gauthier-Villars,1, 173, 1983.

Brasseur, G. and P.C. Simon, Stratospheric chemical and thermal response to long-term variability in solar UV irradiance, J. Geophys. Res., 86, 7343, 1981.

Brasseur, G., M. Janssens, and M. Tavernier, A two-dimensional model of minor constituents in the mesosphere and lower thermosphere, paper presented at the General Assembly of the International Union of Geodesy and Geophysics, Canberra, Australia, 1980.

Brasseur, G., P. De Baets, and A. De Rudder, Solar variability and minor constituents in the lower thermosphere and in the mesosphere, Space Sci. Rev., 34, 377, 1983.

Callis, L. B., and J. E. Nealy, Solar UV variability and its effect on stratospheric thermal structure and trace consituents, Geophys. Res. Lett., 5, 249, 1978a.

Callis, L. B., and J. E. Nealy, The effect of UV variability on stratospheric thermal structure and trace constituents, Space Res., 18, 95, 1978b.

Callis, L.B., M. Natarajan, and J.E. Nealy, Ozone and temperature trends associated with the 11-year solar cycle, Science, 204, 1303, 1979.

Cook, J. W., G. E. Brueckner, and M.E. Hoosier,

Variability of the solar flux in the far ultraviolet 1175-2100A, J. Geophys. Res., 85, 2257, 1980.

Danilov, A. D., and J. Taubenheim, NO and temperature control of the D region, Space Sci. Rev., 34, 413, 1983.

De Baets, P., G. Brasseur, and P. C. Simon, Chemical response of the middle atmosphere to solar variations, Sol. Phys., 74, 349, 1981.

Dickinson, P. H. G., R. C. Bolden, and R.A. Young, Measurement of atomic oxygen in the lower ionosphere using a rocket-borne resonance lamp, Nature, 252, 289, 1974.

Dickinson, P. H. G., N. D. Twiddy, and R. A. Young, Atomic oxygen concentrations in the lower ionosphere, Space Res., 16, 301, 1976.

Dickinson, P. H. G., U. von Zahn, K. D. Baker, and D. B. Jenkins, Lower thermosphere densities of N_2, O and Ar under high latitude winter conditions, J. Atom. Terr. Phys., 47, 283, 1985.

Dymek, M.K., Photochemical model of ion composition and electron density in the ionosphere at 70-300 km, Low Latitude Aeronomical Processes, edited by A.P. Mitra, COSPAR Symp. Ser., vol. 8, p. 115, Pergamon Press, Oxford and New York, 1980.

Ebel, A., Eddy diffusion models for the mesophere and lower thermosphere, J. Atmos. Terr. Phys., 42, 617, 1980.

Fehsenfeld, F.C. and E.E. Ferguson, The origin of water cluster ions in the D region, J. Geophys. Res., 74, 2217, 1969.

Ferguson, E. E., Ion-molecule reactions in the atmosphere, Kinetics of ion-molecule reactions, edited by P. Ausloos, p. 377, Plenum, New York, 1979.

Forbes, J. M., Tidal effects on D and E region ion chemistries, J. Geophys. Res., 86, 1981.

Garcia, R.R. and S. Solomon, A numerical model of the zonally averaged dynamical and chemical structure of the middle atmosphere, J. Geophys. Res., 88, 1379, 1983.

Garcia, R. R. and S. Solomon, The effect of breaking gravity waves on the dynamics and chemical composition of the mesosphere and lower thermosphere, J. Geophys. Res., 90, 3850, 1985.

Garcia, R. R., S. Solomon, R. G. Roble and D. W. Rusch, A numerical response of the middle atmosphere to the 11-year solar cycle, Planet. Space Sci., 32, 411, 1984.

Geller, M. A. and J. C. Alpert, Planetary wave coupling between the troposphere and the middle atmosphere as a possible sun-weather mechanism, J. Atmos. Sci., 37, 1197, 1980.

Goldberg, R. A., Silicon ions below 100 km : A case for SiO_2, Radio Sci., 10, 329, 1975.

Goldberg, R. A. and A. C. Aikin, Studies of positive-ion composition in the equatorial D-region ionosphere, J. Geophys. Res., 76, 8352, 1971.

Goldberg, R. A. and L. J. Blumle, Positive ion composition from a rocket-borne mass spectrometer, J. Geophys. Res., 75, 133, 1970.

Grossman, K. U., Mesospheric water vapour, in Proceedings of the sixth symposium on European rocket and balloon programmes Eur. Space Agency Spec. Publ. (ESA SP-183), 87, 1983.

Heaps, M. G., A parameterization of cosmic ray ionization, Planet. Space Sci., 26, 513, 1978.

Heath, D. F. and M. P. Thekaekara, The solar spectrum between 1200 and 3000 A, in The Solar Output and Its Variation, edited by O. R. White, p. 193, Colorado Associated University Press, Boulder, 1977.

Hinteregger, H. E., Representations of solar EUV fluxes for aeronomical applications, Adv. Space Res., 1, 39, 1981.

Holton, J. R., The influence of gravity wave breaking on the general circulation of the middle atmosphere, J. Atmos. Sci., 40, 2497, 1983.

Hunt, B. G., A Generalized aeronomic model of the mesosphere and lower thermosphere including ionospheric processes, J. Atmos. Terr. Phys., 35, 1755, 1973.

Johnson, F. S. and B. Gottlieb, Eddy mixing and circulation at ionospheric levels, Planet. Space. Sci., 18, 1707, 1970.

Johnson, F. S. and B. Gottlieb, Atomic oxygen transport in the thermosphere, Planet. Space Sci., 21, 1001, 1973.

Keesee, R. G., N. Lee and A. W. Castleman, Jr. Atmospheric negative ion hydration derived from laboratory results and comparison to rocket-borne measurements in the lower ionosphere, J. Geophys. Res., 84, 3719, 1979.

Kopp, E., P. Eberhardt, and U. Herrmann, Summer daytime positive ion composition in the D region above Wallops Island, Space Res., 18, 245, 1978.

Kopp, E. and U. Herrmann, Ion composition in the lower ionosphere, Ann. Geophys. Gauthier Villars, 83, 1984.

Lean, J. L., O. R. White, W. C. Livingstone, D. F. Heath, R. F. Donnelly, and A. Skumanich, A three-component model of the solar flux variability : 145-200 nm, J. Geophys. Res., 87, 10307, 1982.

Lee, L. C., and G. P Smith, Photodissociation and photodetachment of molecular negative ions, III, Ions in $O_2/CH_4/H_2O$ mixtures from 3500 to 8600 A, J. Chem. Phys., 70, 1727, 1979.

Lindzen, R. S., Turbulence and stress owing to gravity wave and tidal breakdown, J. Geophys. Res., 86, 9707, 1981.

Meira, C. G., Jr. Rocket measurements of upper atmospheric nitric oxide and their consequences to the lower ionosphere, J. Geophys. Res., 76, 202, 1971.

Mitra, A. P., Chemistry of middle atmospheric ionization-a review, J. Atmos. Terr. Phys., 43, 737, 1981.

Mount, G. H., G. J. Rottman and J. G. Timothy, The solar spectral irradiance 1200-1550 A at solar maximum, J. Geophys. Res., 85, 4271, 1980.

Murgatroyd, R. J., and F. Singleton, Possible meridional circulations in the stratosphere and mesosphere, Q. J. R. Meteorol. Soc., 87, 125, 1961.

Narcisi, R. S. and A. D. Bailey, Mass spectrometric measurements of positive ions at altitudes from 64 to 112 kilometers, J. Geophys. Res., 70, 3687, 1965.

Natarajan, M., L. B. Callis, and J. E. Nealy, Solar UV variability : effects on stratospheric ozone, trace constituents and thermal structure, Pure Appl. Geophys., 119, 750, 1981.

Nicolet, M., Contribution à l etude de la

structure de l'ionosphère, Mém. Inst. R. Meteorol. Belg., 19, 83, 1945.
Nicolet, M., Changes in atmospheric chemistry related to solar flux variations, in Solar-Terrestrial Influences on Weather and Climate, edited by B. M. McCormac, University of Colorado Press, Boulder, 1983.
Nicolet, M., and A. C. Aikin, The formation of the D region of the ionosphere, J. Geophys. Res., 65, 1469, 1960.
Nicolet, M., and L. Bossy, Relations between solar flux and E-region parameters, AGARD Conf. Proc., 295, 20, 1981.
Offermann, D., H. G. K. Bruckelmann, J. J. Barnett, K. Labitzke, K. M. Torkar, and H. U. Widdel, A scale analysis of the D region winter anomaly, J. Geophys. Res., 87, 8286, 1982.
Paulsen, D. E., R. E. Huffman, and J. C. Larrabee, Improved photoionization rates of $O_2(^1\Delta g)$ in the D region, Radio Sci., 7, 51, 1972.
Penner, J. E., and J. S. Chang, Possible variation in atmospheric ozone related to the 11-year solar cycle, Geophys. Res. Lett., 5, 817, 1978.
Penner, J. E., and J. S. Chang, The relationship between atmospheric trace species variabilities and solar UV variability, J. Geophys. Res., 85, 5523, 1980.
Reid, G. C., Production and loss of electrons in the quiet daytime D region of the ionosphere, J. Geophys. Res., 75, 2551, 1970.
Reid, G. C., Ion chemistry in the D-region, Advances in Atomic and Molecular Physics, vol. 12, edited by D. R. Bates and B. Bederson, 375, Academic, Orlando, Fla., 1976.
Reid, G. C., The production of water cluster positive ions in the quiet daytime D region, Planet. Space Sci., 25, 275, 1977.
Roble, R. G., and B. A. Emery, On the global mean temperature of the thermosphere, Planet. Space Sci., 31, 597, 1983.
Roble, R. G., and M. H. Rees, Time dependent studies of the aurora : Effects of particle precipitation on the dynamic morphology of ionospheric and atmospheric properties, Planet. Space Sci., 25, 991, 1977.
Rottman, G. J., Rocket measurements of the solar spectral irradiance during solar minimum, 1972-1977, J. Geophys. Res., 86, 6697, 1981.
Rottman, G. J., 27-day variations observed in solar UV (120-300 nm) irradiance, Planet. Space Sci., 31, 1001, 1983.
Rowe, J. N., A. P. Mitra, A. J. Ferraro, and H. S. Lee, An experimental and theoretical study of the D-region, II. A Semi-empirical model for mid-latitude D-region, J. Atmos. Terr. Phys., 36, 755, 1974.
Schwentek, H., Regular and irregular behavior of the winter anomaly in ionospheric absorption, J. Atmos. Terr. Phys., 33, 1647, 1971.
Sechrist, Jr., C. F., Theoretical model of the D-region, J. Atmos. Terr. Phys., 34, 1565, 1972.
Sears, R. D., M. G. Heaps, and F. E. Niles, Modeling the ion chemistry of the D-region : A case study based upon the 1966 total solar eclipse, J. Geophys. Res., 86, 10073, 1981.
Smith, G. P., L. C. Lee, P. C. Cosby, J. R. Peterson, and J. T. Moseley, Photodissociation and photodetachment of molecular negative ions, V, Atmospheric ions from 7000 to 8400 A, J. Chem. Phys., 68, 3818, 1978.
Solomon, S., and R. R. Garcia, Transport of thermospheric NO to the upper stratosphere, Planet. Space Sci., 32, 399, 1984.
Solomon, S., P. J. Crutzén, and R. G. Roble, Photochemical coupling between the thermosphere and lower atmosphere, 1, Odd nitrogen from 50 to 120 km, J. Geophys. Res., 87, 7206, 1982a;
Solomon, S., G. C. Reid, R. G. Roble, and P. J. Crutzen, Photochemical coupling between the thermosphere and the lower atmosphere, 2, D region ion chemistry and the winter anomaly J. Geophys. Res., 87, 7221, 1982b.
Stewart, A. I., Photoionization coefficients and photoelectron impact excitation efficiencies in the daytime ionosphere, J. Geophys. Res., 75, 6333, 1970.
Swider, W., Daytime nitric oxide at the base of the thermosphere, J. Geophys. Res., 83, 4407, 1978.
Thomas, L., Recent developments and outstanding problems in the theory of the D region, Radio Sci., 9, 121, 1974.
Thomas, L., Mesospheric temperatures and the formation of water cluster ions in the D region, J. Atmos. Terr. Phys., 38, 1345, 1976.
Thomas, R. J., C. A. Barth, G. J. Rottman, D. W. Rusch, G. H. Mount, G. M. Lawrence, R. W. Sanders, G. E. Thomas, and L. E. Clemens, Ozone density distribution in the mesosphere (50-90 km) measured by the SME limb scanning near infrared spectrometer, Geophys. Res. Lett., 10, 245, 1983.
Thorne, R. M., Influence of relativistic electron precipitation on the lower ionosphere and stratosphere, in B. Grandal B. and J. A. Holtet, Dynamical and Chemical Coupling, edited by D. Reidel, Hingham, Mass., p. 161, 1977.
Tohmatsu, T., and N. Iwagami, Measurement of nitric oxide abundance in the equatorial upper atmosphere, J. Geomagn. Geoelectr., 28, 343, 1976.
Torkar, K. M., and Friedrich, Tests of an ion-chemical model of the D- and lower E-region, J. Atmos. Terr. Phys., 45, 369, 1983.
Weinstock, J. , Non linear theory of gravity waves: Momentum deposition, generalized Rayleigh friction, and diffusion , J. Atmos. Sci., 39, 1698, 1982.
Wisemberg, J., and G. Kockarts, Negative ion chemistry in the terrestrial D region and signal flow graph theory, J. Geophys. Res., 85, 4642, 1980.
Zbinden, PA., MA. Hidalgo, P. Eberhardt, and J. Geiss, Mass spectrometer measurements of the positive ion composition in the D and E regions of the ionosphere, Planet. Space Sci., 23, 1621, 1975.

G. Brasseur and P. De Baets, Institut d'Aéronomie Spatiale de Belgique, 3 Avenue Circulaire, B-1180 Brussels, Belgium.

(Received September 6, 1984;
revised September 11, 1985;
accepted September 12, 1985.)